RESULTS

Effects of chemicals on the migration of cNCCs

Of the 13 chemicals we tested, six chemicals, that is, 13-*cis*-retinoic acid, ethanol, ibuprofen, lead acetate, salicylic acid, and selenate, significantly inhibited the migration of cNCCs at their embryotoxic concentrations. 13-*cis*-Retinoic acid reduced the migration of cNCCs by approximately 13% at concentrations of 3 and 10 μM (Fig. 3A). Ethanol, ibuprofen, salicylic acid and selenate reduced the migration of cNCCs by 10.5% at 195 mM, 15.9% at 2 mM, 8.5% at 3 mM and 16.2% at 150 μM, respectively (Figs. 3B - E).

Lead acetate reduced the migration of cNCCs by 11.6% at 3 μM and by 30.0% at 10 μM in an initial experiment (Fig. 3F). Because evaluation of the toxic effects of lead at low exposure levels is important for human health, two lower concentrations were added stepwise so that the no-observed-effect level could be estimated. Lead acetate reduced the migration of cNCCs significantly by 8.7% at 1 μM; however, the decrease (6.4%) was not significant at 0.1 μM (Fig. 3G).

The remaining seven chemicals, that is, acetaminophen, caffeine, indium, phenytoin, selenite, tributyltin, and valproic acid, had no significant effects on the migration of cNCCs even at high concentrations (Figs. 4A-G). Indium did not affect the migration of cNCCs and tNCCs in the experiments (Fig. 4C). These experiments for indium were performed at a single concentration for cNCCs and tNCCs because indium showed no effects on the migration of cNCCs in a pilot study and because indium has been reported to cause malformation in the caudal part of rat embryos (Nakajima et al. 2008).

Effects of chemicals on the proliferation of cNCCs

Effects on the proliferation of cNCCs were examined in the case of six chemicals (i.e., 13-*cis*-retinoic acid, ethanol, ibuprofen, lead acetate, salicylic acid, and selenate) that showed inhibitory effects on the migration of cNCCs. The effects of tributyltin on cNCC proliferation were also examined because of our interest in another research project. To reduce the number of animals to be used, two chemicals with the same vehicle were examined concomitantly when possible. In the control groups, the actual cell count increased by approximately 50% during the 24-h exposure period.

13-*cis*-Retinoic acid did not significantly reduce the proliferation of cNCCs at concentrations of 3 and 10 µM, the same concentrations at which it inhibited the migration of cNCCs, although the cell count ratio and the cell proliferation ratio were lowered by 2.5% and 9.7%, respectively, at 3 µM compared to the control group (Fig. 5A).

Ethanol, ibuprofen, salicylic acid, and selenate significantly reduced the cell count ratio by 16.3%, 14.1%, 12.3%, and 20.6%, and the cell proliferation ratio by 59.0%, 43.0%, 33.1%, and 55.4%, respectively, at the same concentrations (195 mM, 2 mM, 3 mM, and 150 µM, respectively) at which they inhibited the migration of cNCCs (Fig. 5B - D).

Lead acetate increased the cell count ratio by 2.2% and the cell proliferation ratio by 6.6% at 1 µM concentration, the lowest effective concentration for inhibiting the migration of cNCCs, although these differences were not statistically significant (Fig. 5C).

Tributyltin reduced the cell count ratio by 9.2% and the cell proliferation ratio by 27.0% at 100 nM concentration, although no reduction in the migration of cNCCs was observed (Fig. 5E).

There was no significant correlation between proliferation inhibition and migration inhibition when the reduced migration was plotted against the reduced cell count ratio, suggesting a varied contribution of the latter to the former (Fig. 6).

DISCUSSION

Here, we observed inhibition of the migration of rat cNCCs by six developmentally toxic chemicals including those not previously reported to have the inhibitory effects: ibuprofen, salicylic acid, and selenate. It is speculated that inhibition of the migration of cNCCs results in reduction of the number of cNCCs at their destination tissues. The inhibited migration of cNCCs by itself, however, seems insufficient as a pathogenic mechanism underlying teratogenicity because these chemicals do not necessarily cause similar malformations. It is probable that the inhibited migration of cNCCs that is not accompanied by an excessive cell shortage is compensated by accelerated cell proliferation at their destination tissues. Alternatively, these inhibitory effects may occur differently in the body of embryos.

From the results of the proliferation assay, it is considered that the reduced cell number may contribute to the inhibited migration of cNCCs to varying extents depending on the test chemicals. It is suggested that the migration-inhibitory effects of ethanol, ibuprofen, and selenate are due in part to the reduced number of cNCCs. In contrast, in the case of tributyltin, the reduced cell number did not affect the migration of cNCCs. Chemicals that did not inhibit cell proliferation, for example, 13-*cis*-retinoic acid, and lead acetate, appeared to inhibit the migration of cNCCs independent of the cell number.

13-*cis*-Retinoic acid appeared to more potently inhibit the migration of cNCCs than all-*trans*-retinoic acid, because the inhibitory concentration of the former (3 μM) was found to be lower than that of the latter (10 μM) in our previous study (Usami et al. 2014b). This is inconsistent with the teratogenic potential of the retinoic acids in rats, where 13-*cis*-retinoic acid is less teratogenic because of its faster elimination from the body (Collins et al. 1994). Isolated cNCCs themselves may be more susceptible to

13-*cis*-retinoic acid than all-*trans*-retinoic acid, as suggested by the lower affinity of 13-*cis*-retinoic acid for cytoplasmic retinoid binding proteins, which may enable easy access to the cell nucleus (Rühl et al. 2001).

Ethanol is a well-known teratogen causing craniofacial malformations (Schardein & Macina 2006) and its toxic effects on NCCs have often been investigated. It was previously shown that ethanol caused apoptotic cell death (Yan et al. 2010) and inhibited migration (Shi et al. 2014) of NCCs. In the present study, both reduced cell number and inhibited migration of cNCCs were observed as the effects of ethanol, although the effective concentration of ethanol was relatively higher than those reported in previous studies, probably because of species and strain differences in the susceptibility to ethanol (Wentzel & Eriksson 2008).

Inhibitory effects of ibuprofen and salicylic acid, which are non-steroidal anti-inflammatory drugs (NSAIDs), on the migration of NCCs have not been reported to date. Although these NSAIDs are considered non-teratogenic in humans, their embryotoxic effects, including craniofacial malformations, observed in animal experiments (Joschko et al. 1993; Kosar 1993) may be related to their migration-inhibitory effects on cNCCs.

The migration-inhibitory effects of lead acetate in the present study are consistent with previously reported results for human NCCs derived from embryonic stem cells (Zimmer et al. 2012). In both studies, lead acetate at 1 μM (20 μg/dl) or higher concentrations inhibited the migration of NCCs without reduced cell proliferation. It is noted that this inhibitory concentration is comparable to blood lead levels (40.0 ± 16.5 μg/dl, mean ± SD) in a certain proportion of pregnant women (Ugwuja et al. 2012). Although lead caused craniofacial malformations only in cultured rat embryos (Zhao et al. 1997)

and does not cause major malformations in humans, its migration-inhibitory effects on cNCCs, as a neuronal progenitor, may be related to functional deficiencies such as neurological alterations (Flora et al. 2011).

The effects of the two selenium compounds on the migration of cNCCs were different in the present study; i.e., selenate inhibited the migration of cNCCs while selenite did not. This difference may be related to the difference in malformed optic vesicles and the protein expression changes caused by the selenium compounds in cultured rat embryos; selenate caused enlargement of the optic vesicle (Usami et al. 2008), a destination of migrating cNCCs (Le Douarin & Kalcheim 1999), and increased the phosphorylated form (inactive form) of cofilin 1 (Usami et al. 2008), an actin-binding protein essential for the migration of NCCs (Gurniak et al. 2005), while selenite did not cause either (Usami et al. 2008). It is thus speculated that selenate inhibits the migration of cNCCs through inactivation of cofilin 1, which results in malformation of the optic vesicle.

In this context, it is intriguing that ethanol and indium also increased phosphorylated cofiline 1 in cultured rat embryos (Usami et al. 2014a; Usami et al. 2009). However, indium did not have inhibitory effects on the migration of cNCCs or tNCCs in the present study. This may indicate that the increase in phosphorylated cofilin 1 alone is not a sufficient condition for inhibition of the migration of NCCs, or that it could occur in different embryonic cells.

The proliferation-inhibitory effects of tributyltin on cNCCs without reduced migration may be related to its developmental toxicity; treatment of pregnant rats with tributyltin that caused blood concentrations comparable to those in the present study, reduced the body weights of pups without causing external malformations (Adeeko et al. 2003; Cooke et al. 2008).

It is unknown at present why the proliferation-inhibitory effects of tributyltin were not accompanied by the inhibited migration of cNCCs. It is unlikely that tributyltin increased the migration of cNCCs, compensating its proliferation-inhibitory effects. This is because tributyltin did not have any effects on the migration of cNCCs over the concentration tested even when the neural tube was removed at 18 h of culture and the cNCCs could move more freely during the exposure period (data not shown). Rather, the relatively selective toxicity and accumulation of tributyltin in the mitochondria (Doherty & Irwin 2011) might have no effects on the migration of cNCCs. In any case, no correlation between proliferation inhibition and migration inhibition means that the NCC migration assay can not be replaced by usual cytotoxicity assays based on the cell number and is valuable to investigate the effects of chemicals on the function of NCCs.

While valproic acid did not inhibit the migration of cNCCs in the present study, the effects of valproic acid on the migration of NCCs are controversial. Valproic acid inhibited the migration of human NCCs in a scratch assay (Zimmer et al. 2012), but did not inhibit the migration of chick NCCs in cultured neural tubes (Fuller et al. 2002). Currently available data indicate that the effects of valproic acid on the migration of NCCs seem to depend on the assay method and the species used in which it is used.

For other chemicals (acetaminophen, caffeine, and phenytoin) that did not inhibit the migration of cNCCs, no particular information concerning the involvement of NCCs' malfunction in their developmental toxicity was found, except that acetaminophen did not inhibit the migration of human NCCs either (Zimmer et al. 2012).

In conclusion, it was established that several developmentally toxic chemicals inhibit the migration of cNCCs, which appears differently as craniofacial abnormalities. Mechanistic investigation is needed to understand the variability in the outcomes of the

inhibited migration of cNCCs. Our migration assay method will be useful for this purpose because of its simplicity.

CONFLICT OF INTEREST

The authors declare that there are no conflicts of interest.

ACKNOWLEDGEMENTS

This work was supported by a Health and Labor Science Research Grant from the Ministry of Health, Labour and Welfare in Japan.

REFERENCES

Adeeko A, Li D, Forsyth DS, Casey V, Cooke GM, Barthelemy J, Cyr DG, Trasler JM, Robaire B, Hales BF. 2003. Effects of in utero tributyltin chloride exposure in the rat on pregnancy outcome. Toxicol Sci 74: 407–15.

Collins MD, Tzimas G, Hummler H, Bürgin H, Nau H. 1994. Comparative teratology and transplacental pharmacokinetics of all-*trans*-retinoic acid, 13-*cis*-retinoic acid, and retinyl palmitate following daily administrations in rats. Toxicol Appl Pharmacol 127: 132–44.

Cooke GM, Forsyth DS, Bondy GS, Tachon R, Tague B, Coady L. 2008. Organotin speciation and tissue distribution in rat dams, fetuses, and neonates following oral administration of tributyltin chloride. J Toxicol Environ Health A 71: 384–95.

Doherty JD, Irwin WA. 2011. Organotins (tributyltin and triphenyltin). In: Gupta RC, editor. Reproductive and Developmental Toxicology. Sandiego, California: Elsevier. p. 657–672.

Flora SJS, Pachauri V, Saxena G. 2011. Arsenic, cadmium and lead. In: Gupta RC, editor. Reproductive and Developmental Toxicology. Sandiego, California: Elsevier. p. 415–438.

Fuller LC, Cornelius SK, Murphy CW, Wiens DJ. 2002. Neural crest cell motility in valproic acid. Reprod Toxicol 16: 825–839.

Greenaway JC, Mirkes PE, Walker EA, Juchau MR, Shepard TH, Fantel AG. 1985. The effect of oxygen concentration on the teratogenicity of salicylate, niridazole, cyclophosphamide, and phosphoramide mustard in rat embryos in vitro. Teratology 32: 287–295.

Guest I, Buttar HS, Smith S, Varma DR. 1994. Evaluation of the rat embryo culture system as a predictive test for human teratogens. Can J Physiol Pharmacol 72: 57–62.

Gurniak CB, Perlas E, Witke W. 2005. The actin depolymerizing factor n-cofilin is essential for neural tube morphogenesis and neural crest cell migration. Dev Biol 278: 231–241.

Hall BK. 2009. Neurocristopathies. In: The Neural Crest and Neural Crest Cells in Vertebrate Development and Evolution. 2nd ed. New York: Springer. p. 269–293.

Joschko MA, Dreosti IE, Tulsi RS. 1993. The teratogenic effects of salicylic acid on the developing nervous system in rats in vitro. Teratology 48: 104–114.

Kawakami M, Umeda M, Nakagata N, Takeo T, Yamamura K-I. 2011. Novel migrating mouse neural crest cell assay system utilizing P0-Cre/EGFP fluorescent time-lapse imaging. BMC Dev Biol 11: 68.

Kim S-R, Kubo T, Kuroda Y, Hojyo M, Matsuo T, Miyajima A, Usami M, Sekino Y, Matsushita T, Ishida S. 2014. Comparative metabolome analysis of cultured fetal and adult hepatocytes in humans. J Toxicol Sci 39: 717–23.

Kosar K. 1993. Interaction of ibuprofen with early chick embryogenesis. Pharmazie 48: 207–9.

Le Douarin N, Kalcheim C. 1999. The Neural Crest. 2nd ed. New York: Cambridge University Press.

Lee QP, Juchau MR, Kraft JC. 1991. Microinjection of cultured rat embryos: studies with retinol, 13-cis- and all-trans-retinoic acid. Teratology 44: 313–23.

Menegola E, Broccia ML, Di Renzo F, Massa V, Giavini E. 2004. Relationship between hindbrain segmentation, neural crest cell migration and branchial arch abnormalities in rat embryos exposed to fluconazole and retinoic acid *in vitro*. Reprod Toxicol 18: 121–130.

Nakajima M, Mitsunaga K, Nakazawa K, Usami M. 2008. In vivo/in vitro study in rat embryos on indium-caused tail malformations. Reprod Toxicol 25: 426–32.

Robinson JF, van Beelen VA, Verhoef A, Renkens MFJ, Luijten M, van Herwijnen MHM, Westerman A, Pennings JLA, Piersma AH. 2010. Embryotoxicant-specific transcriptomic responses in rat postimplantation whole-embryo culture. Toxicol Sci 118: 675–85.

Rühl R, Plum C, Elmazar MM, Nau H. 2001. Embryonic subcellular distribution of 13-*cis*- and all-*trans*-retinoic acid indicates differential cytosolic/nuclear localization. Toxicol Sci 63: 82–9.

Schardein JL, Macina OT. 2006. Ethanol. In: Human Developmental Toxicants: Aspects of Toxicology and Chemistry. Boca Raton, Florida: Taylor & Francis. p. 301–322.

Shi Y, Li J, Chen C, Gong M, Chen Y, Liu Y, Chen J, Li T, Song W. 2014. 5-mehtyltetrahydrofolate rescues alcohol-induced neural crest cell migration abnormalities. Mol Brain 7: 67.

Shreiner CM, Zimmerman EF, Wee EL, Scott Jr WJ. 1986. Caffein effects on cyclic AMP levels in the mouse embryonic limb and palate in vitro. Teratology 34: 21–27.

Ugwuja EI, Ibiam UA, Ejikeme BN, Obuna JA, Agbafor KN. 2012. Blood Pb Levels in pregnant Nigerian women in Abakaliki, South-Eastern Nigeria. Environ Monit Assess.

Usami M, Mitsunaga K, Irie T, Miyajima A, Doi O. 2014a. Proteomic analysis of ethanol-induced embryotoxicity in cultured post-implantation rat embryos. J Toxicol Sci 39: 285–92.

Usami M, Mitsunaga K, Irie T, Miyajima A, Doi O. 2014b. Simple in vitro migration assay for neural crest cells and the opposite effects of all-trans-retinoic acid on cephalic- and trunk-derived cells. Congenit Anom (Kyoto) 54: 184–188.

Usami M, Mitsunaga K, Nakazawa K, Doi O. 2008. Proteomic analysis of selenium embryotoxicity in cultured postimplantation rat embryos. Birth Defects Res B Dev Reprod Toxicol 83: 80–96.

Usami M, Nakajima M, Mitsunaga K, Miyajima A, Sunouchi M, Doi O. 2009. Proteomic analysis of indium embryotoxicity in cultured postimplantation rat embryos. Reprod Toxicol 28: 477–88.

Weeks BS, Gamache P, Klein NW, Hinson JA, Bruno M, Khairallah E. 1990. Acetaminophen toxicity to cultured rat embryos. Teratog Carcinog Mutagen 10: 361–71.

Wentzel P, Eriksson UJ. 2008. Genetic influence on dysmorphogenesis in embryos from different rat strains exposed to ethanol in vivo and in vitro. Alcohol Clin Exp Res 32: 874–887.

Winn L. 2002. Evidence for Ras-Dependent Signal Transduction in Phenytoin Teratogenicity. Toxicol Appl Pharmacol 184: 144–152.

Yan D, Dong J, Sulik KK, Chen S. 2010. Induction of the Nrf2-driven antioxidant response by tert-butylhydroquinone prevents ethanol-induced apoptosis in cranial neural crest cells. Biochem Pharmacol 80: 144–9.

Zhao SF, Zhang XC, Zhang LF, Zhou SS, Zhang F, Wang QF, Wang YL, Bao YS. 1997. The evaluation of developmental toxicity of chemicals exposed occupationally using whole embryo culture. Int J Dev Biol 41: 275–282.

Zimmer B, Lee G, Balmer N V, Meganathan K, Sachinidis A, Studer L, Leist M. 2012. Evaluation of developmental toxicants and signaling pathways in a functional test based on the migration of human neural crest cells. Environ Health Perspect 120: 1116–22.

Legends to the figures

Fig. 1. Culture schedule of for the migration and proliferation assays of cephalic neural crest cells (cNCCs)

Neural tubes were excised from the rhombencephalic region of day 10.5 rat embryos and cultured for 48 h to allow the emigration of cNCCs. Chemicals were added to the culture medium at 24 h. In the proliferation assay, the neural tubes were removed from the culture dishes at 18h leaving the cNCCs behind, and the cell nuclei were fluorescently stained before the photography at 48 h.

Fig. 2. Photographs of cephalic neural crest cells (cNCCs) cultured in the migration and proliferation assays

(A) cNCCs cultured in the migration assay are shown with blue polygons connecting the outermost cells for the calculation of the cell migration. (B) cNCCs cultured in the proliferation assay are shown with blue dots (24 h) or stained cell nuclei (48 h) for the determination of the cell count.

Fig. 3. Migration of cephalic neural crest cells (cNCCs) cultured in the presence of developmentally toxic chemicals with migration-inhibitory effects

Migration indices were calculated as the radius ratio from the circular spread of cNCCs at 24 and 48 h of culture. The mean ± standard error of the mean (SEM) values of 6–27 neural tubes are shown. Asterisks indicate statistically significant differences from the corresponding control (*, $p < 0.05$; **, $p < 0.01$; ***, $p < 0.001$; ****, $p < 0.0001$).

Fig. 4. Migration of cephalic neural crest cells (cNCCs) cultured in the presence of

developmentally toxic chemicals without migration-inhibitory effects

Migration indices were calculated as the radius ratio from the circular spread of cNCCs at 24 and 48 h of culture. The mean ± standard error of the mean (SEM) values of 8–16 neural tubes are shown. Effects of indium were examined also in trunk neural crest cells as shown in (C).

Fig. 5. Proliferation of cephalic neural crest cells (cNCCs) cultured in the presence of developmentally toxic chemicals

The cNCCs were counted at 24 and 48h of culture, and the proliferation indices were calculated. The mean ± standard error of the mean (SEM) values of 7–10 neural tubes are shown. Asterisks indicate statistically significant differences from the corresponding control (*, $p < 0.05$; **, $p < 0.01$; ***, $p < 0.001$).

Fig. 6. Plot of the reduced migration versus the reduced cell count ratio of neural crest cells cultured in the presence of developmentally toxic chemicals

The reduced migration and reduced cell count ratio were calculated by subtracting the corresponding data in Figs. 1–3 from 100%. The linear regression line and correlation coefficient (r) for all the plotted data are shown.

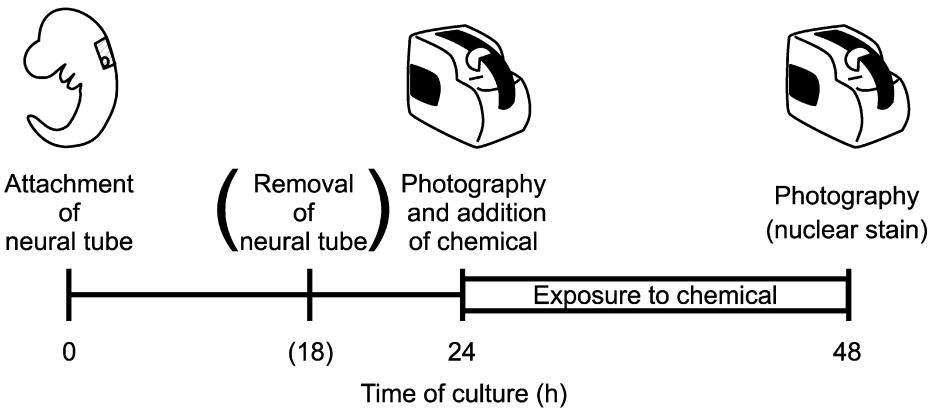

Fig. 1

CGA_12121_F1

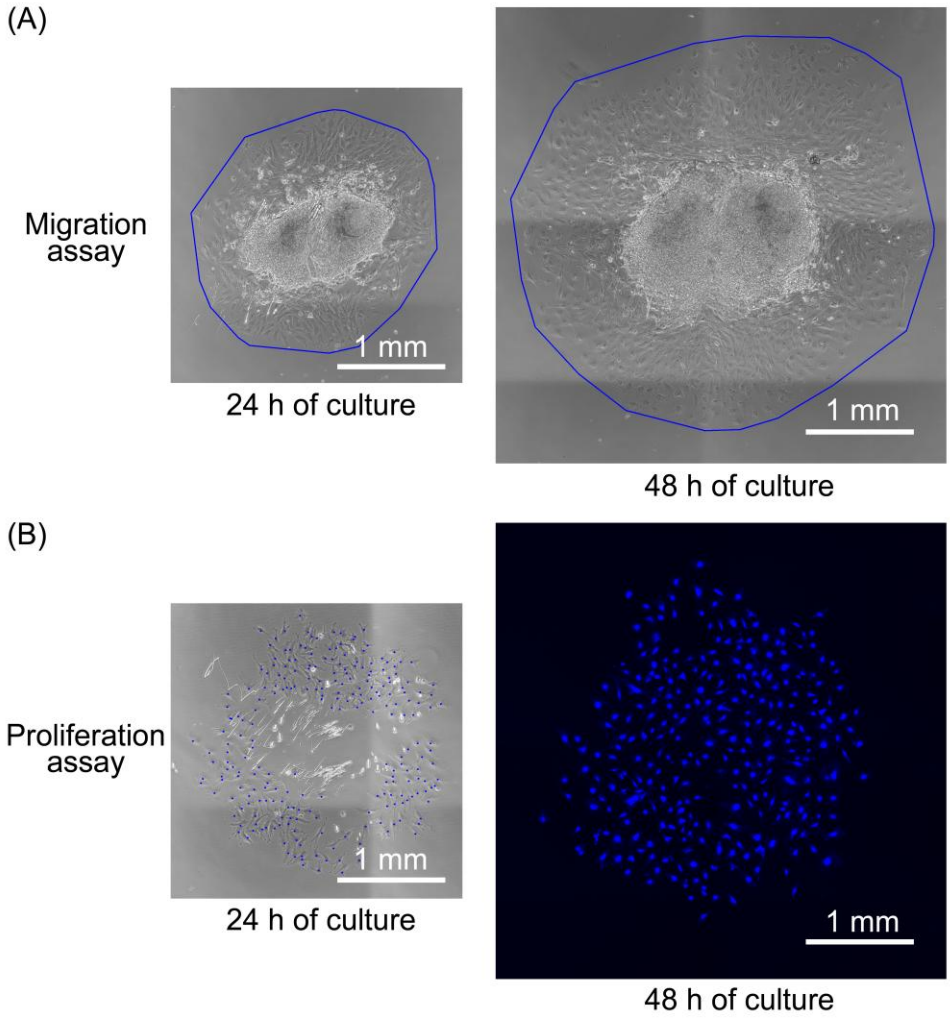

Fig.2

CGA_12121_F2

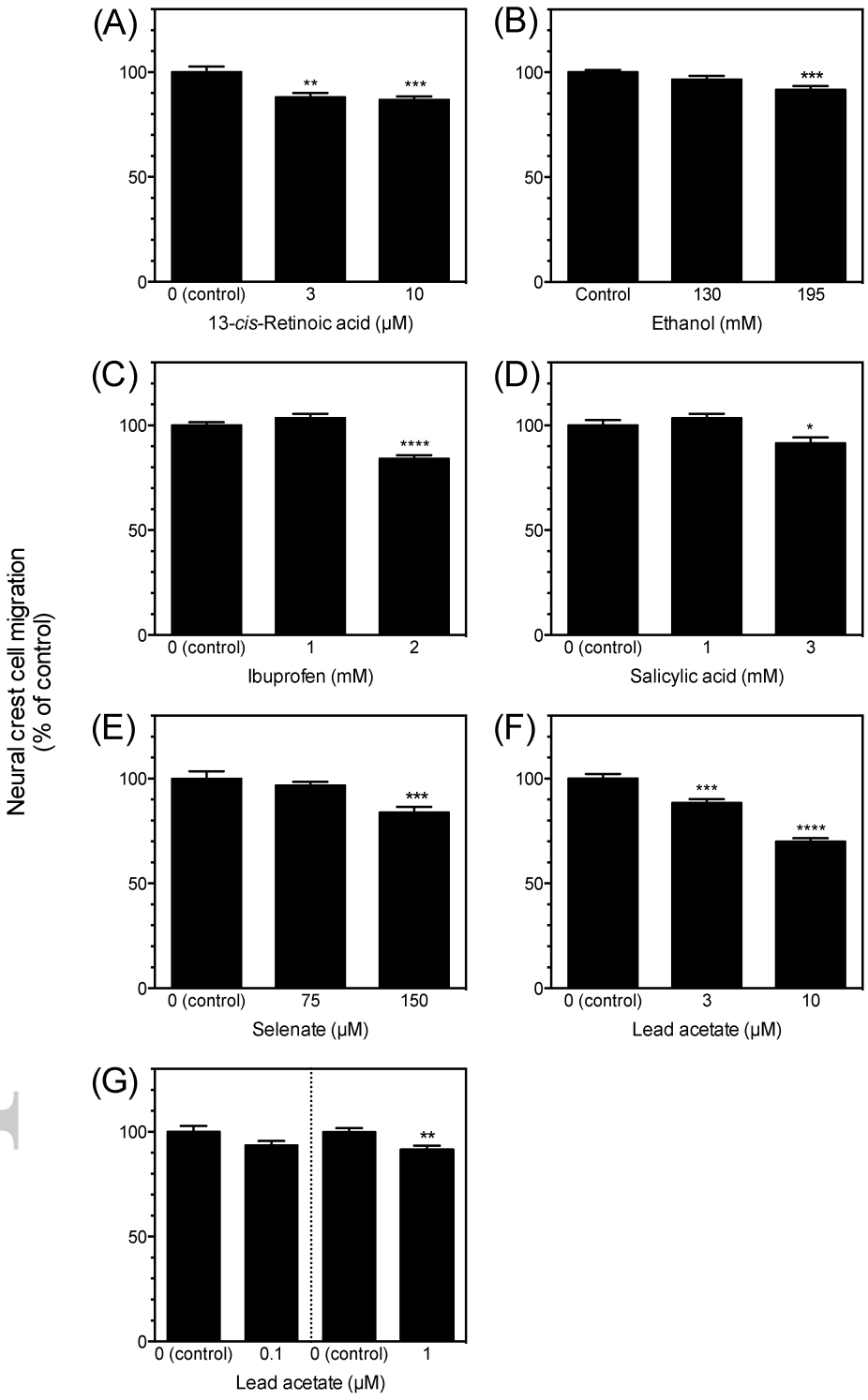

Fig.3

CGA_12121_F3

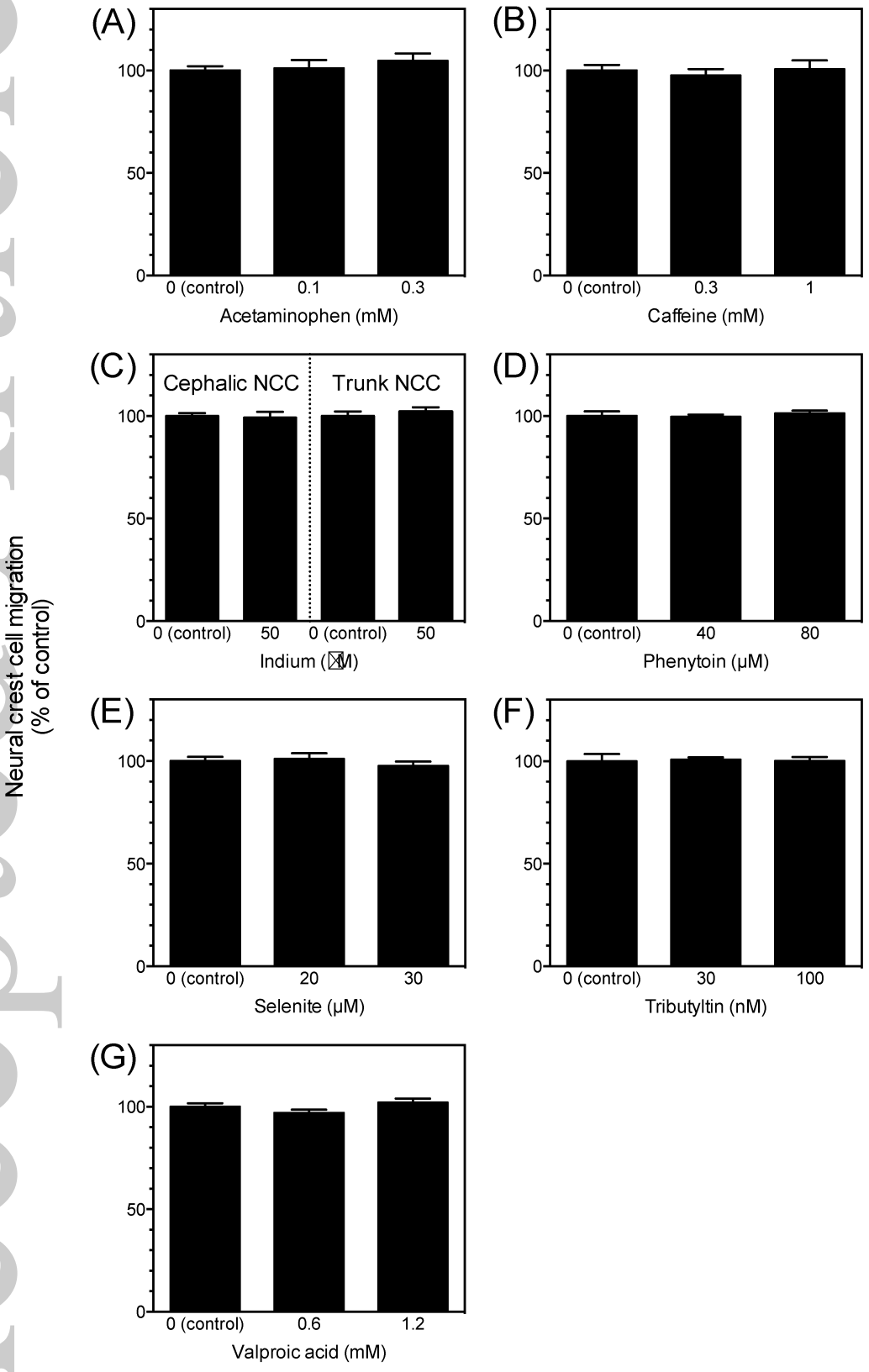

Fig.4

CGA_12121_F4

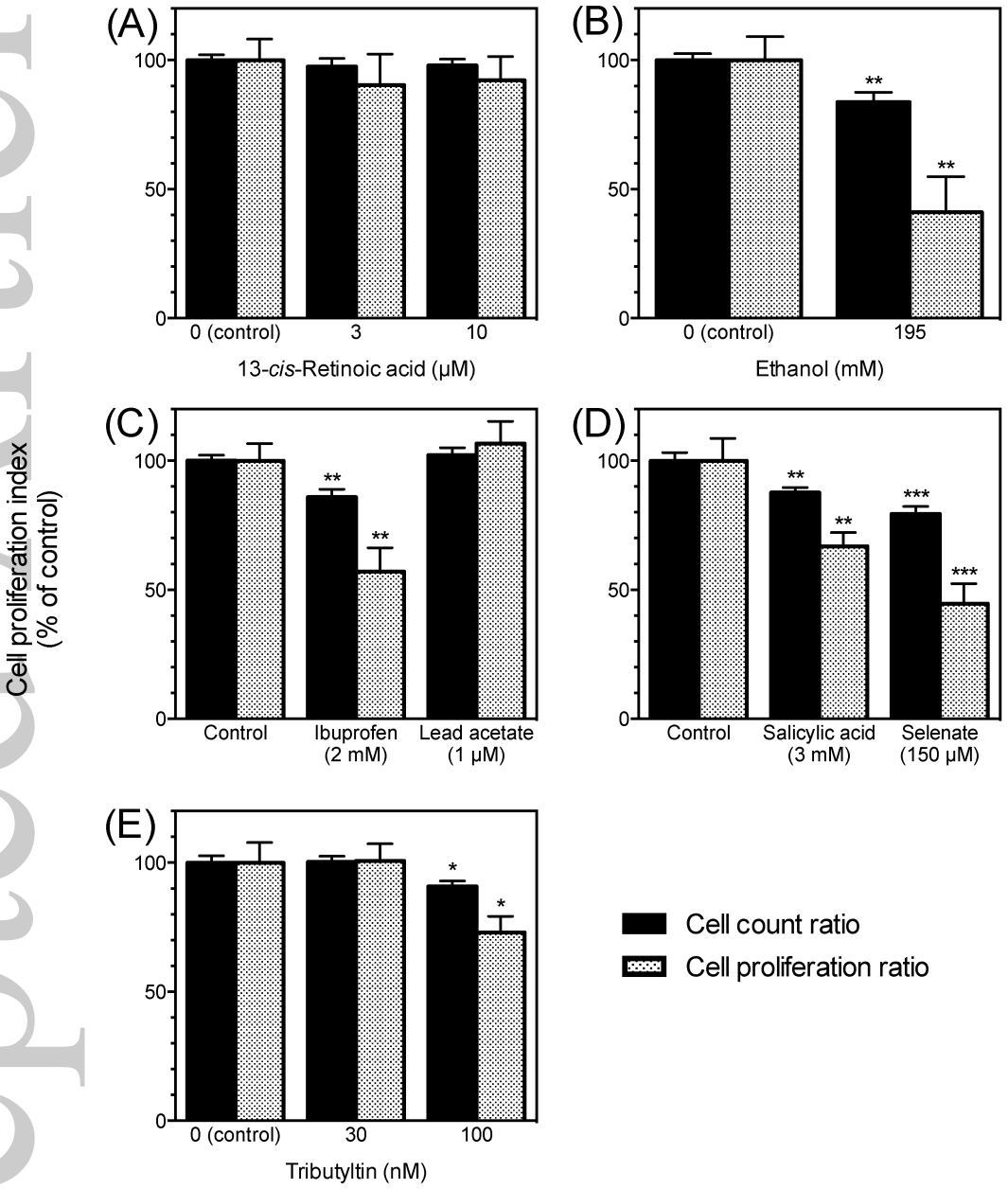

Fig.5

CGA_12121_F5

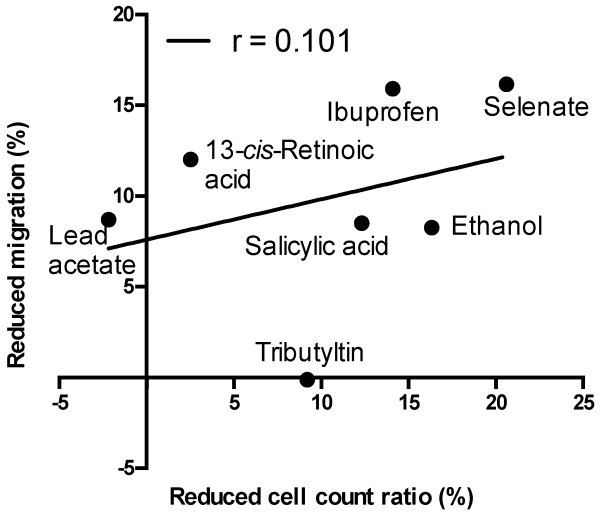

Fig.6

CGA_12121_F6

Neuropharmacology 95 (2015) 479–491

Contents lists available at ScienceDirect

Neuropharmacology

journal homepage: www.elsevier.com/locate/neuropharm

MAM-2201, a synthetic cannabinoid drug of abuse, suppresses the synaptic input to cerebellar Purkinje cells via activation of presynaptic CB1 receptors

Tomohiko Irie [a, *], Ruri Kikura-Hanajiri [b], Makoto Usami [a], Nahoko Uchiyama [b], Yukihiro Goda [c], Yuko Sekino [a, **]

[a] Division of Pharmacology, National Institute of Health Sciences, Tokyo, Japan
[b] Division of Pharmacognosy, Phytochemistry, and Narcotics, National Institute of Health Sciences, Tokyo, Japan
[c] Division of Drugs, National Institute of Health Sciences, Tokyo, Japan

ARTICLE INFO

Article history:
Received 26 June 2014
Received in revised form
18 December 2014
Accepted 20 February 2015
Available online 5 March 2015

Keywords:
Synthetic cannabinoids
MAM-2201
Cannabinoid receptor type 1
Purkinje cell
Cerebellum
Neurotransmitter release

ABSTRACT

Herbal products containing synthetic cannabinoids—initially sold as legal alternatives to marijuana—have become major drugs of abuse. Among the synthetic cannabinoids, [1-(5-fluoropentyl)-1*H*-indol-3-yl](4-methyl-1-naphthalenyl)-methanone (MAM-2201) has been recently detected in herbal products and has psychoactive and intoxicating effects in humans, suggesting that MAM-2201 alters brain function. Nevertheless, the pharmacological actions of MAM-2201 on cannabinoid receptor type 1 (CB1R) and neuronal functions have not been elucidated. We found that MAM-2201 acted as an agonist of human CB1Rs expressed in AtT-20 cells. In whole-cell patch-clamp recordings made from Purkinje cells (PCs) in slice preparations of the mouse cerebellum, we also found that MAM-2201 inhibited glutamate release at parallel fiber-PC synapses via activation of presynaptic CB1Rs. MAM-2201 inhibited neurotransmitter release with an inhibitory concentration 50% of 0.36 μM. MAM-2201 caused greater inhibition of neurotransmitter release than Δ^9-tetrahydrocannabinol within the range of 0.1–30 μM and JWH-018, one of the most popular and potent synthetic cannabinoids detected in the herbal products, within the range of 0.03–3 μM. MAM-2201 caused a concentration-dependent suppression of GABA release onto PCs. Furthermore, MAM-2201 induced suppression of glutamate release at climbing fiber-PC synapses, leading to reduced dendritic Ca^{2+} transients in PCs. These results suggest that MAM-2201 is likely to suppress neurotransmitter release at CB1R-expressing synapses in humans. The reduction of neurotransmitter release from CB1R-containing synapses could contribute to some of the symptoms of synthetic cannabinoid intoxication including impairments in cerebellum-dependent motor coordination and motor learning.

Abbreviations: ACSF, artificial cerebrospinal fluid; AM251, *N*-(piperidin-1-yl)-5-(4-iodophenyl)-1-(2,4-dichlorophenyl)-4-methyl-1*H*-pyrazole-3-carboxamide; CB1R, cannabinoid receptor type 1; CB2R, cannabinoid receptor type 2; CF, climbing fiber; CI, confidence interval; CV, coefficient of variation; DNQX, 6,7-dinitroquinoxaline-2,3-dione; EC50, effective concentration 50%; eCBs, endocannabinoids; EGTA, ethylene glycol tetraacetic acid; EPSC, excitatory postsynaptic current; GFP, green fluorescent protein; hCB1R, human CB1R; HEPES, 4-(2-hydroxyethyl)-1-piperazineethanesulfonic acid; IC50, inhibitory concentration 50%; IEI, inter-event interval; IPSC, inhibitory postsynaptic current; JWH-018, naphthalen-1-yl-(1-pentylindol-3-yl)methanone; LTD, long-term depression; MAM-2201, [1-(5-fluoropentyl)-1*H*-indol-3-yl](4-methyl-1-naphthalenyl)-methanone; mCB1R, mouse CB1R; mIPSC, miniature IPSC; OGB-1, Oregon Green 488 BAPTA-1 hexapotassium salt; P, postnatal day; PC, Purkinje cell; PF, parallel fiber; PPR, paired-pulse ratio; qEPSC, quantal EPSC; THC, tetrahydrocannabinol; TTX, tetrodotoxin; WIN, WIN 55,212-2 mesylate, (*R*)-(+)-[2,3-Dihydro-5-methyl-3-(4-morpholinylmethyl)pyrrolo[1,2,3-de]-1,4-benzoxazin-6-yl]-1-naphthalenylmethanone mesylate.

* Corresponding author. Division of Pharmacology, National Institute of Health Sciences, 1-18-1 Kamiyoga, Setagaya-ku, Tokyo 158-8501, Japan. Tel.: +81 3 3700 9762.
** Corresponding author. Division of Pharmacology, National Institute of Health Sciences, 1-18-1 Kamiyoga, Setagaya-ku, Tokyo 158-8501, Japan. Tel.: +81 3 3700 9692.
E-mail addresses: irie@nihs.go.jp (T. Irie), yukos@nihs.go.jp (Y. Sekino).

http://dx.doi.org/10.1016/j.neuropharm.2015.02.025
0028-3908/

1. Introduction

Marijuana (*Cannabis sativa*) has been widely abused for recreational purposes and contains the psychoactive compound Δ^9-tetrahydrocannabinol (Δ^9-THC) (Taura et al., 2007). Δ^9-THC binds to cannabinoid receptors type 1 and 2 (CB1R and CB2R), which are G protein-coupled receptors. CB1Rs are abundantly expressed in the mammalian brain, whereas CB2Rs are expressed mainly in the immune system (Showalter et al., 1996; Mackie, 2008; Kano et al., 2009). The psychoactive effects of Δ^9-THC are mediated by CB1Rs (Huestis et al., 2001; Monory et al., 2007). Starting in the late 2000s, herbal products containing synthetic cannabinoids, which are chemical compounds produced for the purpose of mimicking the effects of Δ^9-THC, became a major class of drugs of abuse, and are sold as alternatives to marijuana around the world (Auwarter et al., 2009; Vardakou et al., 2010; Seely et al., 2012; Kikura-Hanajiri et al., 2013). Among the synthetic cannabinoids, [1-(5-fluoropentyl)-1*H*-indol-3-yl](4-methyl-1-naphthalenyl)-methanone (MAM-2201, Fig. 1*A*) was recently identified in these herbal products (Moosmann et al., 2012; Derungs et al., 2013; Kikura-Hanajiri et al., 2013; Saito et al., 2013; Uchiyama et al., 2013; Lonati et al., 2014). In humans, abuse of products containing MAM-2201 causes a psychotic state with agitation, aggression, and anxiety, and can cause serious harm to the user including death. These reports imply that MAM-2201 exerts potent pharmacological actions on brain functions and causes psychoactive and intoxicating effects. Nevertheless, it remains unknown whether MAM-2201 activates CB1Rs and how MAM-2201 affects neuronal functions such as synaptic transmission.

Endocannabinoids (eCBs) mediate various types of synaptic plasticity throughout the mammalian brain. eCBs are released from postsynaptic neurons in response to synaptic activity and act in a retrograde manner on presynaptic terminals, to suppress neurotransmitter release (Wilson and Nicoll, 2002; Kano et al., 2009; Regehr et al., 2009). The synaptic effects of eCBs are mediated by presynaptic CB1Rs. In presynaptic terminals, activation of CB1Rs mainly inhibits voltage-gated Ca^{2+} channels coupled to exocytosis, leading to a reduction of neurotransmitter release (Brown et al., 2004; Kushmerick et al., 2004).

Numerous neurophysiological and neuropharmacological studies of CB1Rs have been performed on the cerebellum of rodents, which have well-characterized neuronal circuits and play crucial roles in motor coordination and motor learning (Llinas et al., 2004; Kano et al., 2009). In the cerebellum, Purkinje cells (PCs) are the principal GABAergic neurons and provide the sole output from the cerebellar cortex. PCs receive two types of glutamatergic excitatory inputs, climbing fibers (CFs) and parallel fibers (PFs). CFs arise from the inferior olivary complex. Activation of CF-PC synapses induces strong postsynaptic depolarization, which evokes a dendritic Ca^{2+} transient and complex spikes consisting of a burst of several action potentials (spikelets). PFs are the axons of the granule cells located in the deep layers of the cerebellum and form numerous *en passant* synapses on the spines of distal dendrites of PCs (Llinas et al., 2004). PCs also receive feed-forward inhibition from GABAergic interneurons in the molecular layer of the cerebellar cortex (Mittmann et al., 2005). Neurotransmitter release at CF-PC, PF-PC, and interneuron-PC synapses is suppressed via activation of presynaptic CB1Rs (Kreitzer and Regehr, 2001; Diana et al., 2002; Szabo et al., 2004; Kawamura et al., 2006; Safo et al., 2006). *In vivo* administration of synthetic CB1R agonists in mice impairs cerebellum-dependent motor coordination (DeSanty and Dar, 2001; Patel and Hillard, 2001). Thus, the effects of CB1R agonists on cerebellar functions are well understood. Therefore, the cerebellum is the ideal neuronal circuit to examine the potency of synthetic cannabinoids, whose actions on neuronal functions have not been determined.

Here, using whole-cell patch-clamp recordings, we investigated activity of MAM-2201 in human CB1R (hCB1R)-expressing AtT-20 cells, and then the effects of MAM-2201 on synaptic transmission in slice preparations of the mouse cerebellum. We found that MAM-2201 acted as an agonist of hCB1Rs and inhibited excitatory transmitter release at PF-PC synapses via activation of presynaptic CB1Rs. MAM-2201 decreased the synaptic transmission more strongly than Δ^9-THC within the range of 0.1–30 μM and naphthalen-1-yl-(1-pentylindol-3-yl)methanone [JWH-018, Fig. 1*B*, one of the most popular and potent synthetic cannabinoids detected in the herbal products (Atwood et al., 2010)], within the range of 0.03–3 μM. Furthermore, MAM-2201 induced presynaptic suppression of CF-PC synapses, leading to a reduction in the number of spikelets in complex spikes and to attenuated dendritic Ca^{2+} transients in PCs.

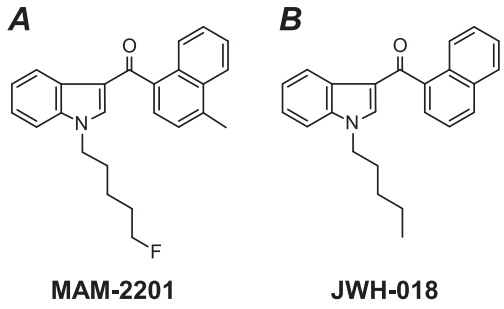

Fig. 1. The chemical structures of [1-(5-fluoropentyl)-1*H*-indol-3-yl](4-methyl-1-naphthalenyl)-methanone (MAM-2201, *A*) and naphthalen-1-yl-(1-pentylindol-3-yl) methanone (JWH-018, B).

2. Materials and methods

2.1. Cannabinoid-related compounds

MAM-2201 (Fig. 1*A*) and JWH-018 (Fig. 1*B*) were purchased from Cayman Chemical (Ann Arbor, MI, USA). (*R*)-(+)-[2,3-Dihydro-5-methyl-3-(4-morpholinylmethyl)pyrrolo[1,2,3-de]-1,4-benzoxazin-6-yl]-1-naphthalenylmethanone mesylate [WIN55,212-2 (WIN), a CB1R and CB2R agonist] and *N*-(Piperidin-1-yl)-5-(4-iodophenyl)-1-(2,4-dichlorophenyl)-4-methyl-1*H*-pyrazole-3-carboxamide (AM251, a CB1R antagonist) were purchased from Wako Pure Chemical Industries (Osaka, Japan) and Tocris Bioscience (Bristol, UK), respectively. Δ^9-THC was purchased from Cerilliant (Round Rock, TX, USA). These compounds were dissolved in dimethylsulfoxide as stock solutions. In electrophysiological recordings from AtT-20 cells and from cerebellar PCs, the final concentrations of dimethylsulfoxide in extracellular solutions were maintained at 0.1 and 0.3% (v/v), respectively. WIN was used as a positive control, because WIN has been used in many studies to suppress neurotransmitter release at PF-, CF-, and interneuron-PC synapses via activation of presynaptic CB1Rs (Kreitzer and Regehr, 2001; Diana et al., 2002; Safo and Regehr, 2005; Kawamura et al., 2006).

2.2. Heterologous expression of CB1R in AtT-20 cells

AtT-20 cells were obtained from JCRB Cell Bank (Osaka, Japan) and were maintained in Ham's F-10 medium (GIBCO, Grand Island, NY) supplemented with 10% horse serum (GIBCO), 2.5% fetal bovine serum (GIBCO), and a mixture of penicillin and streptomycin solution (100 unit/mL and 100 mg/mL, respectively; GIBCO) in a 5% CO_2 incubator at 37 °C. The cells were plated onto grass coverslips coated with poly-D-lysine (Sigma–Aldrich, St Louis, MO) for gene transfection. hCB1R (SC111611; Origene, Rockville, MD; NCBI Reference Sequence: NM_016083.3) (Bruno et al., 2014) or mouse CB1R (mCB1R, MC206086; Origene; GenBank: BC079564.1) cDNAs, and green fluorescent protein (GFP) vector were cotransfected into the cells in a 9:1 M ratio using Lipofectamine LTX (Invitrogen, Carlsbad, CA) according to the manufacturer's instructions. Fluorescence of GFP was regarded as an indicator of transfected cells. Whole-cell patch-clamp recordings were made from the GFP-positive cells 20–48 h after transfection. The expression of CB1R proteins was confirmed by immunostaining with the combination of rabbit polyclonal anti-CB1R antibody (1:2000 dilution, CB1-Rb-Af380, Frontier Institute, Hokkaido, Japan) and AlexaFluor 568-conjugated goat anti-rabbit IgG secondary antibody (5 μg/mL, A-11011; Invitrogen) according to the methods described previously (Irie et al., 2014).

The immunofluorescence signal was observed under a confocal microscope (A1R; Nikon, Tokyo, Japan; Fig. 2A).

2.3. Electrophysiological recordings from AtT-20 cells

AtT-20 cells were transferred to a recording chamber and continuously perfused at 2 mL/min with high-K^+ extracellular solution containing (in mM): 87 NaCl, 60 KCl, 2 $CaCl_2$, 1 $MgCl_2$, 10 D-glucose, and 10 4-(2-hydroxyethyl)-1-piperazineethanesulfonic acid (HEPES) (pH adjusted to 7.4 with NaOH). The concentration of KCl was raised compared to normal extracellular solution to increase amplitudes of inwardly rectifier potassium currents (Mackie et al., 1995). All experiments were performed at 25 ± 1 °C. The cells were visualized by Nomarski optics and a near infrared-CCD camera (C3077-79; Hamamatsu Photonics, Hamamatsu, Japan) with a 40 × 0.8 NA numerical aperture water-immersion objective lens (Olympus, Tokyo, Japan) on an upright microscope (BX51WI; Olympus). GFP-positive cells were visualized and selected using epifluorescence optics (Olympus).

Patch pipettes were made from borosilicate glass capillaries (GC150F-100; Harvard Apparatus, Holliston, MA) and had a resistance of 3–5 MΩ when filled with a potassium gluconate-based internal solution containing (in mM): 125 K-gluconate, 10 KCl, 3 $MgCl_2$, 0.1 ethylene glycol tetraacetic acid (EGTA), 5 Na_2-ATP, 5 Na_2-phosphocreatine, 0.3 Na_2-GTP, and 10 HEPES (pH adjusted to 7.3 with KOH). Whole-cell patch-clamp recordings were performed from GFP-positive cells, and inward currents were evoked by applying voltage steps from a holding potential of −25 mV to −110 mV for 200 ms in voltage-clamp conditions. Membrane capacitance was calculated from the transient current evoked by applying a small voltage step (−5 mV, 20 ms duration) from a holding potential of −25 mV (Irie et al., 2006). Series resistance was compensated electronically by 70–90%, and the liquid junction potential (−5 mV) was corrected off-line.

Data were collected with Molecular Devices (Sunnyvale, CA) hardware and software (Multiclamp 700B, Digidata 1440A, Clampex 10.3) as described previously (Irie et al., 2014), and analyzed using Clampfit 10.3 software (Molecular Devices) and Igor Pro 6 software (Wavemetrics, Lake Oswego, OR) with the added import functionality provided by ReadPclamp XOP of the NeuroMatic software package (http://www.neuromatic.thinkrandom.com/). Representative current traces are shown after averaging four consecutive traces. To obtain inward current densities induced by MAM-2201 or WIN, the amplitudes of the current were normalized to membrane capacitances (picoamperes per picofarad, Fig. 2C). The densities were plotted as a function of the concentration and fit with the sigmoidal function, $Y = Bottom + (Top - Bottom)/(1 + 〖10〗^{(LogEC50 - X)*Hillslope})$, using GraphPad Prism 5 (GraphPad Software, San Diego, CA).

2.4. Cerebellar slice preparation and electrophysiological recordings from PCs

ICR mice of either sex [postnatal day (P) 20–57 for Figs. 3–5 and Table 1; P14–20 for Figs. 6 and 7, and Table 2] were used according to the guidelines for animal use of the National Institute of Health Sciences. Cerebellar slices were prepared as described previously with some modifications (Shuvaev et al., 2011). Briefly, mice were anesthetized with halothane and decapitated. Parasagittal slices of the cerebellum (200-μm thick) were prepared using a microslicer (PRO7, Dosaka, Kyoto, Japan) in ice-cold, cutting solution containing (in mM): 234 sucrose, 2.5 KCl, 1.25 NaH_2PO_4, 10 $MgSO_4$, 0.5 $CaCl_2$, 26 $NaHCO_3$, 11 glucose, and bubbled with 5% CO_2/95% O_2. The slices were then allowed to recover for 1 h at room temperature in artificial cerebrospinal fluid (ACSF) solution containing (in mM): 120 NaCl, 2.5 KCl, 2 $CaCl_2$, 1 $MgCl_2$, 1.25 NaH_2PO_4, 26 $NaHCO_3$, 17 glucose, 0.4 ascorbic acid, 3 myo-inositol, 2 sodium pyruvate, and bubbled with 5% CO_2/95% O_2. In electrophysiological recordings, ascorbic acid, myo-inositol, and sodium pyruvate were omitted.

Cerebellar slices were transferred to a recording chamber, and continuously perfused at 2 mL/min with ACSF at 25 ± 1 °C (Figs. 3–6 and Table 1) or near physiological temperature (34 ± 1 °C; Fig. 7 and Table 2). Electrophysiological recordings were done using the same equipment described above. Excitatory and inhibitory postsynaptic currents (EPSCs and IPSCs) were recorded in the presence of 100 μM picrotoxin (a $GABA_A$ receptor antagonist, Tocris Bioscience) and 40 μM 6,7-dinitroquinoxaline-2,3-dione (DNQX, an AMPA/kainate receptor antagonist, Tocris Bioscience), respectively. Patch pipettes had a resistance of 2–3 MΩ when filled with pipette solutions. A CsCl-based and the K-gluconate-based internal solutions were used for voltage- (Figs. 3–6 and Table 1) and current-clamp recordings (Fig. 7 and Table 2), respectively. The CsCl-based solution contained (in mM): 120 CsCl, 20 K-gluconate, 15 tetraethylammonium-Cl, 3 $MgCl_2$, 5 EGTA, 5 Na_2-ATP, 5 Na_2-phosphocreatine, 0.3 Na_2-GTP, 5 QX-314, and 10 HEPES (pH adjusted to 7.3 with CsOH). The liquid junction potentials (CsCl-based, −4 mV; K-gluconate-based, −10 mV) were corrected off-line.

Somatic whole-cell patch-clamp recordings were performed from PCs in lobules IV to VIII. PF-PC EPSCs and IPSCs were evoked by electrical stimulation of the molecular layer and recorded at the holding potential of −80 mV. CF-PC EPSCs and complex spikes were evoked by the stimulation of the granule cell layer. CF-PC EPSCs were recorded at a holding potential of −10 mV to decrease the driving force for cations through ionotropic glutamate receptors. The stimuli (100- to 200-μs pulses, 20–80 V amplitude) were performed with an ACSF-filled patch pipette (tip diameter, 10–15 μm for molecular layer stimulation and 2–3 μm for the granule cell layer) and applied at 0.1 Hz. In some experiments, paired-pulse stimulation (50 ms inter-stimulus intervals) was done to calculate the paired-pulse ratio (PPR), which is an index of the change of neurotransmitter release from presynaptic terminals (Zucker and Regehr, 2002; Irie and Ohmori, 2008). When postsynaptic currents were recorded, series resistance was monitored by applying small voltage steps (−10 mV, 20-ms duration), and the records were discarded if the resistance varied more than 25%. Quantal EPSCs (qEPSCs) from PFs and CFs were elicited by electrical stimulation (0.1 Hz) with PCs held at −80 mV and with $CaCl_2$ in ACSF replaced with equimolar $SrCl_2$ (Xu-Friedman and Regehr, 1999). Miniature IPSCs (mIPSCs) were recorded at a holding potential of −80 mV in the presence of 40 μM DNQX and 1 μM tetrodotoxin (TTX; Wako Pure Chemical Industries). In the start of current-clamp recordings, resting membrane potentials of PCs were adjusted at −60 to −70 mV by current injection to prevent spontaneous firing, and series resistance was compensated for using bridge balance and capacitance neutralization. Intrinsic membrane properties were examined by square-wave current injection (500-ms duration, Table 2). Input resistance was measured from averaged voltage responses evoked by small hyperpolarizing currents (−20 pA). Threshold current and threshold potential were measured by depolarizing current injections (from 0 pA to 200 pA, 20 pA increment). The maximum rate of rise and maximum rate of fall of action potentials and spike height were calculated from the first action potential waveform evoked at the threshold current. Firing frequency was obtained from the number of spikes observed during the current injection.

qEPSCs and mIPSCs were detected off-line using the template search function in the Clampfit 10.3 software. To analyze qEPSCs, data from 200 to 1600 ms after the stimulus artifact were used. Average cumulative probability histograms were obtained as follows: first, qEPSCs or mIPSCs were recorded more than 300 events from each cell in the presence or absence of MAM-2201. Then, for each cell, the amplitudes and inter-event intervals were binned, and individual cumulative probability histograms were plotted. Finally, these histograms were averaged. Representative EPSC and IPSC traces are shown after averaging four to six consecutive traces, and stimulus artifacts are truncated. EPSC and IPSC amplitudes were obtained by averaging six consecutive records. The coefficient of variation (CV), which is another index of the change of neurotransmitter release from presynaptic terminals, was calculated from 18 consecutive EPSC or IPSC traces (Korn and Faber, 1991). The inhibitory concentration 50% (IC50) values of the cannabinoid-related compounds against neurotransmitter release at PF-PC synapses were calculated as follows: control PF-PC EPSC amplitude was obtained from the averaged EPSCs recorded for 3 min before application of the synthetic cannabinoids. PF-PC EPSC amplitude in the presence of the cannabinoids was done from the EPCSs recorded for 8 to 10 min after the application, normalized to the control values, and plotted as a function of the concentration. The data were fit with the sigmoidal function, $Y = 100/(1 + 〖10〗^{(LogIC50 - X)*Hillslope})$ (Table 1). The reasons for using PF-PC synapses for measurement of IC50s were as follows: PF-PC synapses exhibit more stable synaptic transmission than interneuron-PC synapses (Vincent and Marty, 1996), they are more sensitive to CB1R agonists, and they express CB1R proteins more abundantly than CF-PC synapses (Kawamura et al., 2006).

2.5. Simultaneous recordings of Ca^{2+} transients and complex spikes

Current-clamp recordings were done from PCs using the K-gluconate-based intracellular solution in which EGTA was replaced with 100 μM Oregon Green 488 BAPTA-1 hexapotassium salt (OGB-1; Invitrogen, Carlsbad, CA) in the presence of picrotoxin. PC somata and dendrites were dialyzed with the pipette solution for 30 min to obtain a stable intracellular concentration of OGB-1. Confocal imaging was then performed with a Nipkow disk confocal scanner unit (CSU-10; Yokogawa Electric, Tokyo, Japan) attached to the Olympus BX51WI microscope with the 40× objective lens. A 488 nm beam from a diode laser (Yokogawa Electric) for excitation was coupled to the scanner unit through an optical fiber. Fluorescence was detected via a 520 nm long-path filter using an EMCCD camera (iXon3 DU897; Andor Technology, Belfast, Northern Ireland). The pixels were binned 2 × 2 on the chip, and images were acquired at 25.8 Hz. Complex spikes were evoked at 0.1 Hz, and the electrophysiological recordings were synchronized with the acquisition of time-lapse fluorescent images. The number of spikelets in complex spikes was obtained from average value of five to seven consecutive traces. The imaging experiments were controlled and analyzed using Andor iQ2 software (Andor Technology). Three to five consecutive time-lapse images were averaged and used for analysis. The regions of interests were set on primary dendrites (approximately between 20 and 100 μm from the center of the cell body, Fig. 7Ca). Fluorescence changes were background-corrected and expressed as $\Delta F/F_0$, where F_0 is the fluorescence intensity when the cells were at rest, and ΔF is the absolute values of fluorescence changes during activity. Integration of Ca^{2+} transients was performed over 2 s from the onset.

All data other than EC50s or IC50s are provided as the means ± standard deviation. EC50s and IC50s are expressed as the best-fit values with 95% confidence interval (CI; Table 1). *n* indicates the number of experiments. Statistical significance was tested using paired *t*-tests test unless otherwise stated (significance, $p < 0.05$).

3. Results

3.1. MAM-2201 acts as an agonist of hCB1Rs and mCB1Rs

To examine whether MAM-2201 activates CB1Rs, we expressed hCB1R or mCB1R cDNAs in murine tumor line AtT-20. Because

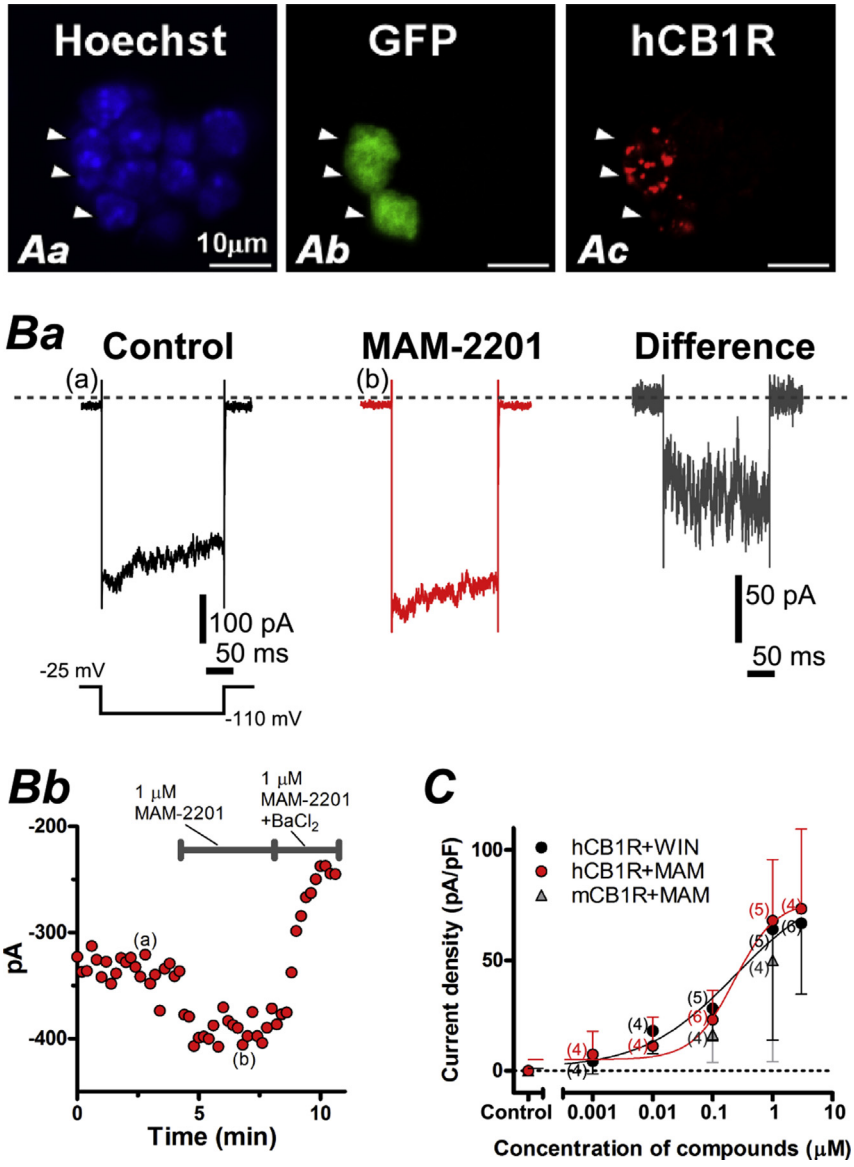

Fig. 2. Heterologous expression of cannabinoid receptor type 1 (CB1R) cDNAs in AtT-20 cells. A, Immunofluorescence images of AtT-20 cells transfected with human CB1R (hCB1R) and green fluorescent protein (GFP) cDNAs. Cell nuclei were stained with Hoechst 33342 (1 μg/mL, Dojindo, Kumamoto, Japan; Aa). Arrowheads indicate GFP and hCB1R double positive cells. Proteins of hCB1Rs were visualized by immunolabelling with rabbit anti-CB1R antibody and AlexaFluor 568-conjugated anti-rabbit secondary antibody (Ac). B, Representative data recorded from hCB1R-expressing cell. Ba, Inward currents were evoked by applying voltage steps from a holding potential of −25 mV to −110 mV for 200 ms. In trace (a) and (b), averages of four consecutive responses are shown. These traces correspond to the responses at time points marked (a) or (b) in Bb. The holding current level is shown by a dotted line. Bb, Time course of mean inward currents. Each point represents an averaged value obtained from four consecutive records. C, Concentration-dependent increases of inward current densities induced by MAM-2201 or (*R*)-(+)-[2,3-Dihydro-5-methyl-3-(4-morpholinylmethyl)pyrrolo[1,2,3-de]-1,4-benzoxazin-6-yl]-1-naphthalenylmethanone mesylate [WIN55,212-2 (WIN)]. To obtain current densities, amplitudes of inward current induced by MAM-2201 or WIN were normalized to membrane capacitances (picoamperes per picofarad). The densities were plotted as a function of the concentration and fit with the sigmoidal function, $Y = \text{Bottom} + (\text{Top} - \text{Bottom})/(1 + 〚10〛^{\hat{}}(\text{LogEC50} - X)*\text{Hillslope})$, where EC50 is effective concentration 50%. Here and in the following figures, error bars and the numbers in parentheses indicate standard deviation and the number of experiments, respectively.

application of CB1 agonists on AtT-20 cells expressing CB1Rs activates inward rectifier potassium currents, activities of compounds against CB1Rs can be determined using this heterologous expression system (Mackie et al., 1995; Felder et al., 1998). Whole-cell patch clamp recordings were done from hCB1R or mCB1R-expressing cells, and inward currents were evoked by applying hyperpolarizing voltage pulses (Fig. 2*B*). Bath application of MAM-2201(1 μM) increased the amplitude of inward current within 5 min (Fig. 2*Bb*). Subsequent application of low concentration of Ba^{2+} (200 μM $BaCl_2$), which blocks inward rectifier potassium currents (Hagiwara et al., 1976), markedly reduced the inward currents. This indicates that, in addition to MAM-2201-induced currents, MAM-2201-independent inward rectifier potassium currents were simultaneously blocked (Dousmanis and Pennefather, 1992). The time course of the induced current, obtained by subtracting the currents before from those after the application of MAM-2201, showed slow activation at the beginning of voltage pulse (Fig. 2*Ba*, Difference). This property is characteristic of activation of G-protein coupled potassium channels (Kubo et al., 1993). Fig. 2*C* shows the concentration-dependent increase of current

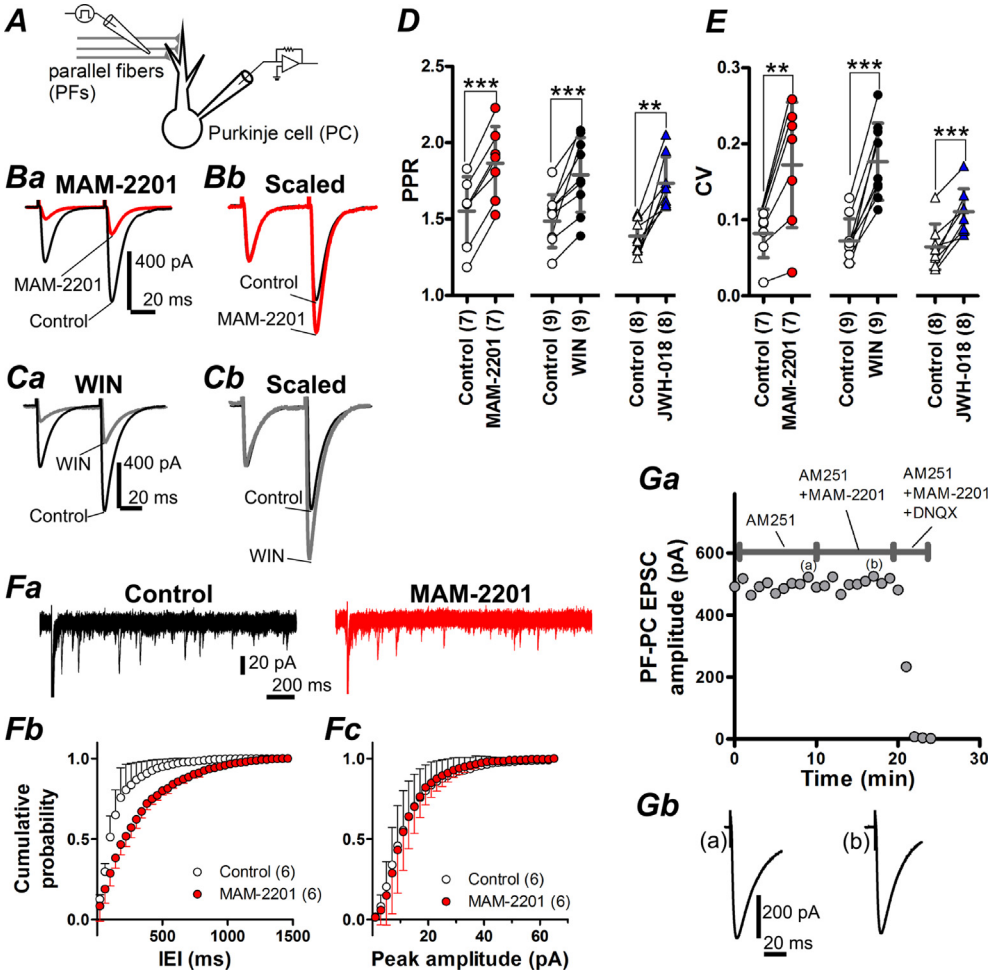

Fig. 3. MAM-2201 inhibits synaptic transmission at parallel fiber (PF)-Purkinje cell (PC) synapses presynaptically via activation of presynaptic CB1Rs. *A*, Experimental configuration for Fig. 3*B*–*G* and 4. *B*, PF-induced excitatory postsynaptic currents (EPSCs) were evoked with pairs of stimuli (50 ms interval) under control conditions (Control) or in the presence of 10 μM MAM-2201 (MAM-2201). The holding potential was −80 mV. Picrotoxin (100 μM) was added to the extracellular artificial cerebrospinal fluid (ACSF) to block $GABA_A$ receptor-mediated inhibitory postsynaptic currents (IPSCs). The first EPSC peak in MAM-2201 was reduced to 21.9% of control. In each trace, averages of six trials are shown. In the right panel, the EPSC evoked by the first stimulus in MAM-2201 is scaled to the amplitude of the first EPSC in Control. MAM-2201 increased paired-pulse facilitation (*Bb*). Stimulus artifacts are truncated. *C*, Same as in *A*, but in the presence of 10 μM WIN. In *Ca*, the first peak in WIN was reduced to 24.1% of control. In the right panel, the EPSC evoked by the first stimulus in WIN is scaled to the amplitude of the first EPSC in Control. *D* and *E*, Summary of paired-pulse ratio (PPR, *D*) and coefficient of variation (CV, *E*) of PF-PC EPSCs before and after application of MAM-2201, WIN, or JWH-018 (10 μM in all groups). Here and in the following figures, the statistical significance was tested using paired *t*-tests unless otherwise stated (significance, $p < 0.05$). $^{**}p < 0.01$ and $^{***}p < 0.001$. *F*, To isolate quantal EPSCs (qEPSCs) from PFs, asynchronous neurotransmitter release from PF terminals was evoked by stimulating PFs in the presence of Sr^{2+} (2 mM, see Materials and Methods). *Fa*, Five superimposed traces before (Control) and after application of MAM-2201. Asynchronously released quanta are seen as downward current deflections. Synchronous PF-PC EPSCs are truncated. *Fb* and *Fc*, Average cumulative probability histograms of inter-event interval (IEI, *Eb*, bin width: 40 ms) and peak amplitude (*Ec*, bin width: 2 pA) of PF-PC qEPSCs. *Ga*, Time course of peak PF-PC EPSC amplitudes in the presence of *N*-(Piperidin-1-yl)-5-(4-iodophenyl)-1-(2,4-dichlorophenyl)-4-methyl-1*H*-pyrazole-3-carboxamide (AM251, 5 μM). Each point represents an averaged value obtained from six consecutive records. MAM-2201 (10 μM) had no detectable effect on the amplitude. Additional application of 6,7-dinitroquinoxaline-2,3-dione (DNQX, 40 μM) abolished PF-PC EPSCs completely. *Gb*, Traces show normalized PF-PC EPSC responses at time points marked (a) and (b) in *Ga*.

densities induced by MAM-2201 or WIN in CB1R-expressing cells. Interestingly, in hCB1R-expressing cells, MAM-2201 increased current densities in a concentration-dependent manner (Fig. 2*C*, red circles) with an EC50 of 0.230 μM (95% CI, 0.0384–1.37 μM). Similar responses were obtained by application of WIN (Fig. 2*C*, black circles; EC50 = 0.234 μM; 95% CI, 0.410 × 10^{-3}-140 μM), which was consistent with previous report (Mackie et al., 1995). In the presence of AM251 (5 μM, a CB1R antagonist), MAM-2201 (1 μM) did not induce the inward currents (−2.38 ± 7.23 pA/pF, $n = 6$). In cells transfected with GFP alone, MAM-2201 (1 μM) did not elicit any changes (1.55 ± 6.78 pA/pF, $n = 5$). In mCB1R-expressing cells, MAM-2201 induced concentration-dependent increase in the current density (Fig. 2*C*, gray triangles). These results demonstrate that MAM-2201 activates hCB1Rs and mCB1Rs.

3.2. MAM-2201 inhibits synaptic transmission presynaptically via activation of presynaptic CB1Rs at PF-PC synapses in mouse cerebellum

We tested the effects of MAM-2201 on neurotransmitter release at PF-PC synapses and the involvement of CB1Rs (Fig. 3), and compared the potency of MAM-2201 with that of WIN, JWH-018, and Δ^9-THC (Fig. 4 and Table 1). Whole-cell patch-clamp recordings were performed from somata of PCs in mouse cerebellar slices under voltage-clamp conditions, and PF-PC EPSCs were evoked by electrical stimulation of PFs in the molecular layer in the presence of picrotoxin. The recording configuration is illustrated in Fig. 3*A*. As shown in Fig. 3*B*, bath application of MAM-2201 (10 μM, 8 min) significantly decreased the first EPSC amplitude

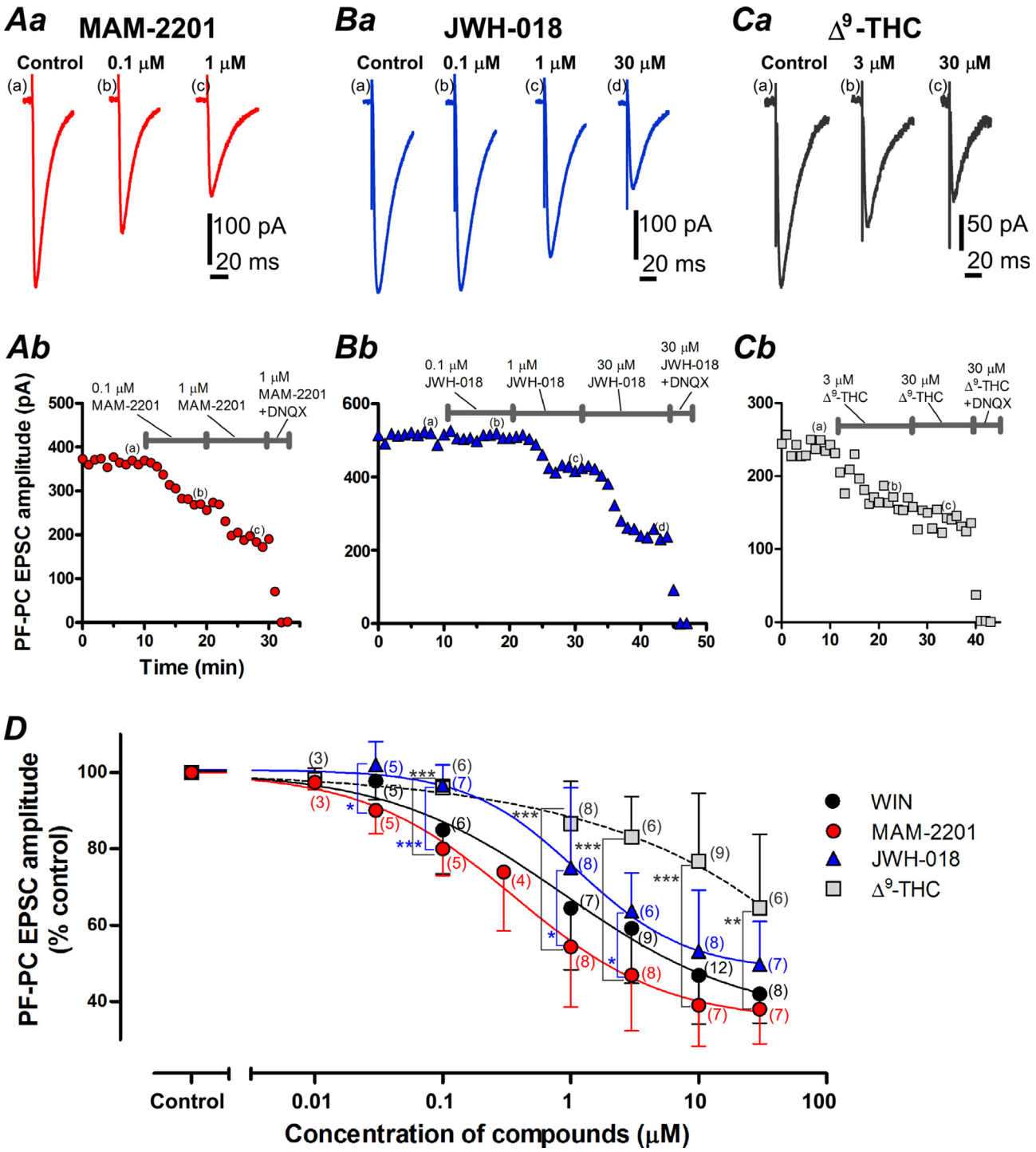

Fig. 4. MAM-2201 is a more potent inhibitor than Δ^9-tetrahydrocannabinol (Δ^9-THC) and JWH-018 at PF-PC synapses. *Aa*, Representative PF-PC EPSC traces recorded in control conditions, or in 0.1 or 1 μM MAM-2201. These traces show normalized PF-PC EPSC responses at time points marked (a), (b), or (c) in *Ab*. *Ab*, Time course of peak amplitudes of PF-PC EPSCs. Each point represents an averaged value obtained from six consecutive records. *Ba*, Representative PF-PC EPSC traces recorded in control conditions, or in 0.1, 1, or 30 μM JWH-018. These traces correspond to the responses at time points marked (a), (b), (c), or (d) in *Bb*. *Bb*, Time course of peak amplitudes of PF-PC EPSCs. *C*, Representative PF-PC EPSC traces recorded in control conditions, or in 3, or 30 μM Δ^9-THC. These traces correspond to the responses at time points marked (a), (b), or (c) in *Cb*. *Cb*, Time course of the peak amplitudes. In *Aa*, *Ba*, and *Ca*, stimulus artifacts are truncated. *D*, Concentration-dependent decreases of PF-PC EPSC amplitudes induced by cannabinoid-related compounds. Control PF-PC EPSC amplitude was obtained from averaged PF-PC EPSCs recorded for 3 min before the application of the compounds. PF-PC EPSC amplitudes in the presence of these compounds were recorded for 8–10 min after application, normalized to the control values, and plotted as a function of concentration (Fig. 4*C*). Each plot was fit with a sigmoidal function, $Y = 100/(1 + [10]^{[(LogIC50 - X)*Hillslope]})$, where IC50 is inhibitory concentration 50%. $^*p < 0.05$, $^{**}p < 0.01$, and $^{***}p < 0.001$ by unpaired *t*-tests test.

(39.0 ± 10.8% of control value, $n = 7$, $p < 0.001$). To investigate whether the effects of MAM-2201 on PF-PC EPSC amplitude were mediated by presynaptic mechanisms, PPR and CV analyses were performed. MAM-2201 (10 μM) significantly increased PPR (Fig. 3*Bb* and *D*) and CV (Fig. 3*E*), indicating a decrease in presynaptic neurotransmitter release. WIN (10 μM, 8-min application) induced a similar decrease in PF-PC EPSC amplitude and a parallel increase in the PPR and CV (Fig. 3*C–E*). MAM-2201 (10 μM) also

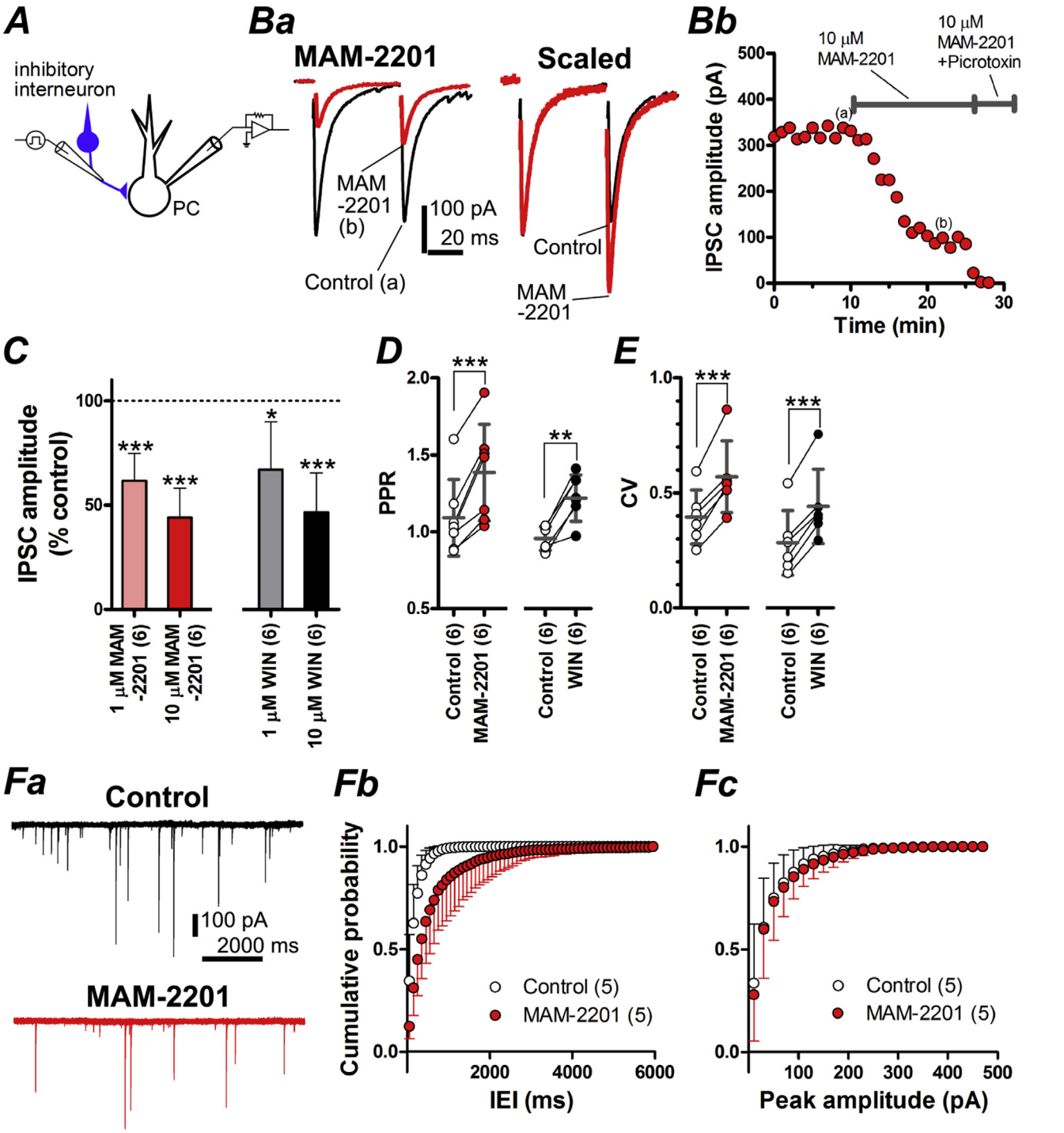

Fig. 5. MAM-2201 reduces GABAergic synaptic transmission at interneuron-PC synapses via presynaptic mechanisms. *A*, Experimental configuration for Fig. 5*B–E*. *Ba*, Averaged current traces of IPSCs in control conditions (Control) and 10 μM MAM-2201. These traces show normalized IPSC responses at time points marked (a) and (b) in *Bb*. IPSCs were evoked with pairs of stimuli (50 ms interval) in the presence of 40 μM DNQX and were recorded as inward currents because of the use of the CsCl-based internal solution. The holding potential was −80 mV, and stimulus artifacts were blanked for clarity. The first peak in MAM-2201 was reduced to 28.0% of control. In the right panel, the first IPSC in MAM-2201 is scaled to the amplitude of the first IPSC in Control (Scaled), showing a clear increase of PPR. *Bb*, Time course of peak amplitudes of the first IPSC. Each point represents an averaged value obtained from six consecutive records. *C*, Concentration-dependent decreases of peak amplitude of IPSC by MAM-2201 and WIN. IPSC amplitudes were normalized to the control value (=baseline responses) and expressed as a percentage of control. $*p < 0.05$ and $***p < 0.001$. *D* and *E*, Summary of PPR (*D*) and CV (*E*) of IPSCs before and after application of MAM-2201 and WIN (10 μM in both groups). $**p < 0.01$. *F*, Miniature IPSCs (mIPSCs) recorded in the presence of tetrodotoxin (TTX, 1 μM) and DNQX. *Fa*, Five superimposed traces before (Control) and after application of MAM-2201. mIPSCs appear as downward current deflections. *Fb* and *Fc*, Average cumulative probability histograms of IEI (*Fb*, bin width: 100 ms) and peak amplitude (*Fc*, bin width: 20 pA) of mIPSCs.

decreased PF-PC qEPSC frequency [Inter-event interval (IEI), Control: 194.0 ± 24.1 ms, MAM-2201: 288.7 ± 30.2 ms, $p < 0.001$, $n = 6$, Fig. 3*Fa* and *Fb*] without affecting PF-PC qEPSC amplitude (peak amplitude, Control: 18.9 ± 2.1 pA, MAM-2201: 18.6 ± 4.3 pA, $p = 0.860$, $n = 6$, Fig. 3*Fa* and *Fc*). In the absence of MAM-2201, amplitudes of PF-PC EPSCs did not show significant changes during 45-min recording under condition in which series resistance was stable (105.2 ± 10.5% of control, $n = 7$, $p = 0.271$).

Table 1
IC50s of synthetic cannabinoids against PF-PC EPSCs.

	WIN	MAM-2201	JWH-018
IC50 (μM) [95% CI (μM)][a]	0.890 [0.296-2.679]	0.363 [0.193-0.681]	1.121 [0.551-2.282]
Relative IC50	1.00	0.41	1.25

[a] Data are provided as the best-fit values with 95% confidence intervals (CI).

To examine whether MAM-2201 altered postsynaptic responses by activating presynaptic CB1Rs, MAM-2201 was bath-applied to the cerebellar slices in the presence of AM251 (5 μM). MAM-2201 did not induce any change of PF-PC EPSC amplitude in the presence of AM251 (Fig. 3*G*, 102.2 ± 6.0% of control, $n = 5$, $p = 0.443$). Subsequent application of DNQX (40 μM) abolished PF-PC EPSCs, demonstrating that glutamatergic synaptic transmission was indeed evoked, and bath application of these chemicals was successful (Fig. 3*Ga*). Taken together, these results indicate that the MAM-2201-induced changes are mediated by a decrease in presynaptic neurotransmitter release from PF terminals via activation of presynaptic CB1Rs.

3.3. MAM-2201 is a more potent inhibitor of PF-PC synapses than Δ^9-THC and JWH-018

Fig. 4*A–C* show representative traces of PF-PC EPSCs in the presence of MAM-2201 (Fig. 4*A*), JWH-018 (Fig. 4*B*), or Δ^9-THC (Fig. 4*C*), respectively. The inhibitory effect of MAM-2201 on PF-PC

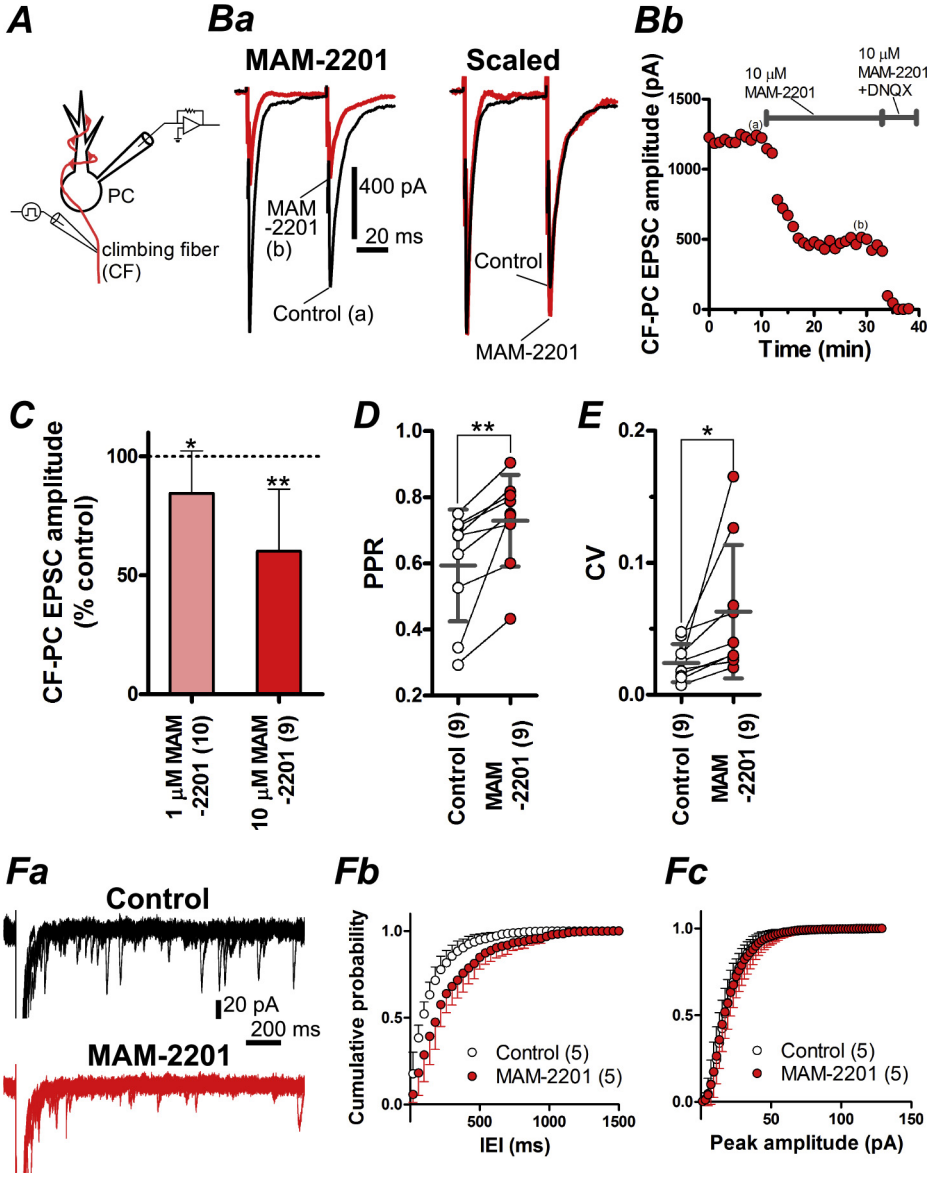

Fig. 6. MAM-2201-mediated presynaptic inhibition at climbing fiber (CF)-PC synapses. *A*, Experimental configuration for Fig. 6*B–F* and 7. *Ba*, Averaged current traces of CF-PC EPSCs in control (Control) and 10 μM MAM-2201. These traces show normalized CF-PC EPSC responses at time points marked (a) and (b) in *Bb*. CF-PC EPSCs were evoked with pairs of stimuli (50 ms interval) in the presence of 100 μM picrotoxin. PCs were held at −10 mV to reduce the driving force for AMPA receptor-mediated currents. Stimulus artifacts were truncated for clarity. The first peak in MAM-2201 was reduced to 38.4% of control. In the right panel, the first CF-PC EPSC in MAM-2201 is scaled to the amplitude of the first CF-PC EPSC of control (Scaled). *Bb*, Time course of peak amplitudes of first CF-PC EPSC. Each point represents an averaged value obtained from six consecutive records. *C*, Concentration-dependent decreases of the peak amplitudes of CF-PC EPSCs by MAM-2201. CF-PC EPSC amplitudes were expressed as a percentage of control. *$p < 0.05$ and **$p < 0.001$. *D* and *E*, Summary of PPR (*D*) and CV (*E*) of CF-PC EPSCs before and after application of MAM-2201 (10 μM). *F*, CF-PC qEPSCs in the presence of picrotoxin and Sr^{2+} (2 mM $SrCl_2$). The qEPSCs were recorded at a holding potential of −80 mV. *Fa*, Five superimposed traces before (Control) and after application of MAM-2201. Synchronous CF-PC EPSCs are truncated. *Fb* and *Fc*, Average cumulative probability histograms of IEI (*Fb*, bin width: 40 ms) and peak amplitude (*Fc*, bin width: 2 pA) of CF-PC qEPSCs.

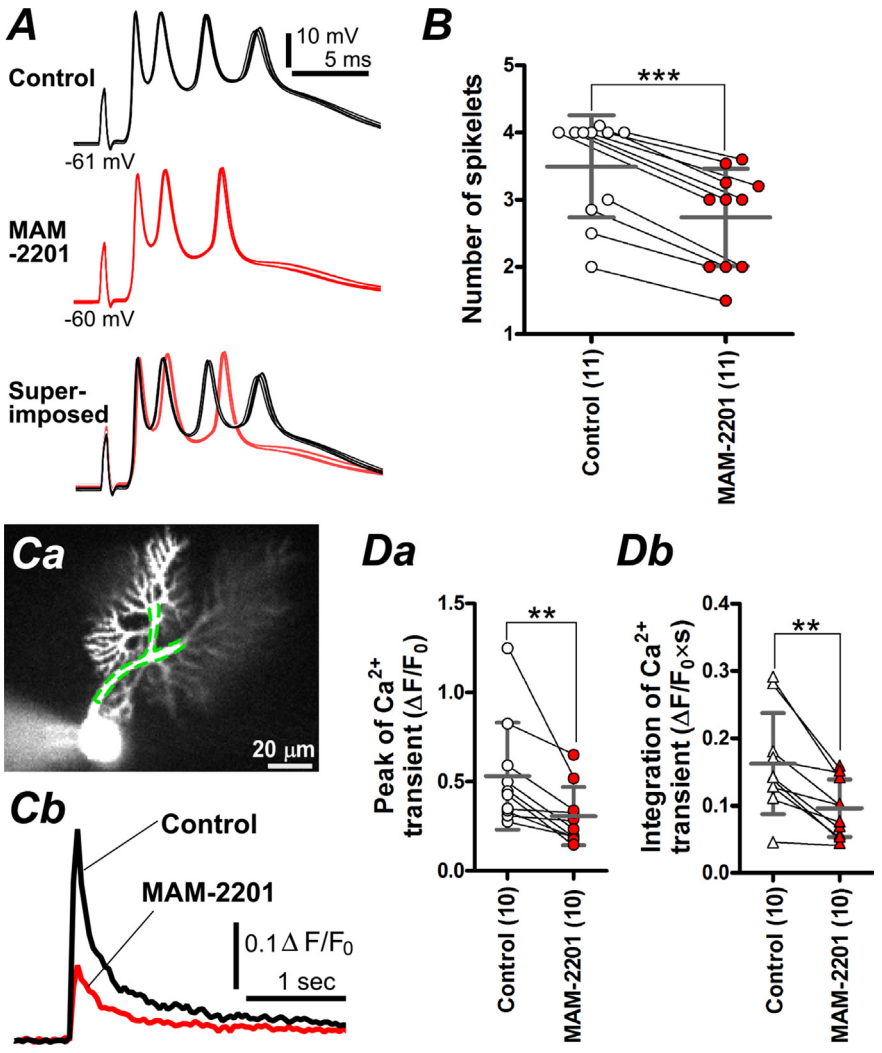

Fig. 7. MAM-2201 reduces the number of spikelets in complex spikes and dendritic Ca^{2+} transients evoked by CF stimulation. *A–D*, Simultaneous recordings of complex spikes and dendritic Ca^{2+} transients. *A*, Representative superimposed traces of complex spikes (5 traces) evoked by stimulation of CFs (0.1 Hz) in the presence of picrotoxin at near physiological temperature (34 ± 1 °C). The K-gluconate-based intracellular solution containing Oregon Green 488 BAPTA-1 hexapotassium salt (OGB-1, 100 μM) was used for current-clamp recordings. At the start of the recording, the resting membrane potential was adjusted around −60 to −70 mV by current injection to prevent spontaneous firing. MAM-2201 (10 μM, 10 min) reduced the number of spikelets (4 spikelets in Control; 3 spikelets in MAM-2201). Superimposed traces reveal delay and reduction of spikelets in MAM-2201. *B*, Summary of average number of spikelets before and after application of MAM-2201 (10 μM). ***$p < 0.001$. *C*, A dendritic Ca^{2+} transient induced by CF stimulation. Intracellular Ca^{2+} measurement in *C* was simultaneously performed while recording the complex spikes in *A*. *Ca*, Representative confocal image of PC loaded with OGB-1 via a patch pipette. Area indicated by dotted line represents region of interest used for the calculation of the dendritic Ca^{2+} transients. *Cb*, Representative Ca^{2+} transients in control and MAM-2201 (10 μM). F_0 is the fluorescence intensity when the cells were at rest, and ΔF is the absolute values of fluorescence changes during activity. *Da* and *Db*, Summary of Ca^{2+} transient peaks (*Da*) and integration of Ca^{2+} transients (*Db*). The integration was performed for 2 s from the onset. **$p < 0.01$.

EPSC amplitude was first detectable at 0.03 μM (Fig. 4*D*, 90.1 ± 6.1% of control, $n = 5$, $p < 0.05$), and became more apparent at higher concentrations. Application of 0.1 μM MAM-2201 was sufficient to induce a clear reduction [trace (b) in Fig. 4*Aa*, 71.9% of control], and subsequent administration of 1 μM MAM-2201 induced further decrease [trace (c) in Fig. 4*Aa*, 51.0% of control]. On the other hand, 0.1 μM JWH-018 did not have detectable effects on PF-PC EPSCs [trace (b) in Fig. 4*Ba*, 99.0% of control; 0.1 μM JWH-018 in Fig. 4*D*, $n = 7$, $p = 0.096$]. Higher concentrations of JWH-018 were required to reduce PF-PC EPSC amplitude [trace (c) in Fig. 4*Ba*, 1 μM, 81.0% of control; trace (d) in Fig. 4*Ba*, 30 μM, 44.2% of control]. Application of Δ^9-THC, which acts as a partial agonist of CB1Rs (Shen and Thayer, 1999; Luk et al., 2004), decreased amplitude of PF-EPSCs obviously at 3 μM [trace (b) in Fig. 4*C*, 68.6% of control], but subsequent administration of 30 μM Δ^9-THC did not induce a clear reduction [trace (c) in Fig. 4*C*, 57.0% of control]. Δ^9-THC (30 μM) significantly increased PPR and CV ($n = 6$, data not shown), indicating a decrease in presynaptic neurotransmitter release. Fig. 4*D* shows the concentration-dependent decreases of PF-PC EPSC amplitude induced by cannabinoid-related compounds. MAM-2201 decreased PF-PC EPSCs more potently than JWH-018 within the range of 0.03–3 μM (Fig. 4*D*, blue triangles (in the web version), $p < 0.05$ and $p < 0.01$ by unpaired *t*-tests test) and Δ^9-THC within the range of 0.1–30 μM (Fig. 4*D*, gray squares, $p < 0.001$ by unpaired *t*-tests test). Application of WIN decreased PF-PC EPSC amplitude to 64.5 ± 0.16% ($n = 7$) of the control value at a concentration of 1 μM and to 46.8 ± 0.13% ($n = 12$) at 10 μM (Fig. 4*D*, WIN). These results are comparable to the previous reports using cerebellar slice preparations from rodents (see Discussion) (Levenes et al., 1998; Takahashi and Linden, 2000; Kawamura et al., 2006). The IC50s of the synthetic cannabinoids against PF-PC EPSCs are summarized in Table 1, and indicate that the rank order of potency for inhibition is MAM-

Table 2
MAM-2201 did not affect intrinsic membrane properties of PCs.

	Control ($n = 10$)	10 μM MAM-2201 ($n = 10$)	p value
Resting membrane potential (mV)	−65.3 ± 3.2	−66.0 ± 3.5	0.43
input resistance (MΩ)	113 ± 51	101 ± 34	0.29
Threshold current (pA)	71.0 ± 39.5	77.8 ± 7.4	0.24
Threshold potential (mV)	−45.4 ± 5.6	−44.9 ± 6.4	0.50
Spike height (mV)	44.9 ± 6.4	45.4 ± 47.6	0.71
Maximum rate of rise (V/s)	114 ± 40	131 ± 37	0.20
Maximum rate of fall (V/s)	−93.0 ± 17	−89.2 ± 15.8	0.14
Firing frequency at 200 pA (Hz)	33.0 ± 18.4	34.4 ± 20.5	0.77
Firing frequency at 500 pA (Hz)	72.6 ± 29.8	77.8 ± 42.1	0.68

Young mice (P14–20) and the K-gluconate-based internal solution were used for the experiments. Current-clamp recordings were performed at near physiological temperature (34 ± 1 °C).
Data are provided as the means ± standard deviation, and n = number of experiments.

2201 > WIN > JWH-018. These findings are consistent with our unpublished data on the IC50s for these synthetic cannabinoids, measured by a binding assay for human recombinant CB1Rs (see Discussion). IC50 of Δ^9-THC was not able to be calculated due to ambiguous fitting. These results demonstrate that MAM-2201 is a more potent inhibitor of PF-PC synaptic transmission than JWH-018 and Δ^9-THC.

3.4. MAM-2201 inhibits GABAergic synaptic transmission at inhibitory interneuron-PC synapses via presynaptic mechanisms

PCs receive feed-forward inhibition from GABAergic inhibitory interneurons lying in the molecular layer of the cerebellar cortex (Llinas et al., 2004), and this inhibition shapes the spike output of PCs (Mittmann et al., 2005). To explore how MAM-2201 modulates this inhibitory synaptic input, we recorded GABAergic synaptic transmission at inhibitory interneuron-PC synapses and examined the effects of MAM-2201 on inhibitory transmission. As shown in Fig. 5*B*, 10 μM MAM-2201 decreased the first IPSC amplitude (MAM-2201 in Fig. 5*Ba* and *Bb*; Fig. 5*C*, $n = 6$, $p < 0.001$), and a similar reduction was observed by 1 μM MAM-2201, indicating the MAM-2201-induced decrease was concentration-dependent (Fig. 5*C*, MAM-2201). MAM-2201 (10 μM) significantly increased PPR and CV (Scaled in Fig. 5*Ba*, *D* and *E*, MAM-2201), and these increases were comparable to those obtained by WIN (10 μM, Fig. 5*D* and *E*, WIN). Moreover, MAM-2201 (10 μM) decreased mIPSC frequency (IEI, Control: 451.2 ± 464.1 ms, MAM-2201: 718.8 ± 542.9 ms, $p < 0.05$, $n = 5$, Fig. 5*Fa* and *Fb*) without affecting mIPSC amplitude (peak amplitude, Control: 45.3 ± 22.3 pA, MAM-2201: 48.3 ± 24.1 pA, $p = 0.53$, $n = 5$, Fig. 5*Fa* and *Fc*). These results demonstrate that MAM-2201 inhibits GABAergic synaptic transmission at interneuron-PC synapses via presynaptic mechanisms.

3.5. MAM-2201-mediated presynaptic inhibition at CF-PC synapses reduces the number of spikelets in complex spikes and dendritic Ca^{2+} transients in PCs

Activation of CFs produces AMPA receptor-mediated strong postsynaptic depolarization and evokes an all-or-none spike with multiple peaks (spikelets), called "complex spikes" in the soma (Llinas et al., 2004). Complex spikes are accompanied by a large, dendritic Ca^{2+} transient, which plays a crucial role in producing long-term depression (LTD) at PF-PC synapses (Konnerth et al., 1992). At CF terminals, activation of presynaptic CB1Rs by WIN reduces glutamate release (Maejima et al., 2001). To examine how presynaptic modulation by MAM-2201 at CF-PC synapses affects the waveforms of complex spikes and CF-induced dendritic Ca^{2+} transients, we first confirmed presynaptic inhibition by MAM-2201 at CF-PC synapses (Fig. 6), and then performed simultaneous recordings of complex spikes and intracellular Ca^{2+} transients (Fig. 7).

First, CF-PC EPSCs were recorded at the holding potential of −10 mV in the presence of picrotoxin (Fig. 6*B–E*). To improve the space clamp in dendrites, young mice (P14–20) were used for the following experiments. This was because CF innervation of PCs is almost matured at this age (Hashimoto and Kano, 2013), and their dendrites are compact compared with those of adult (~P57) mice (McKay and Turner, 2005). As shown in Fig. 6*B* and *C*, bath application of MAM-2201 (1 or 10 μM) reduced CF-PC EPSC amplitude in a concentration-dependent manner. This reduction was accompanied by significant increases in PPR and CV (10 μM MAM-2201; Scaled in Fig. 6*Ba*, *C* and *D*). Moreover, MAM-2201 (10 μM) decreased CF-PC qEPSC frequency (IEI, Control: 176.5 ± 40.3 ms, MAM-2201: 234.5 ± 51.1 ms, $p < 0.01$, $n = 5$, Fig. 6*Fa* and *Fb*) without affecting CF-PC qEPSC amplitude (peak amplitude, Control: 22.5 ± 2.7 pA, MAM-2201: 22.0 ± 4.0 pA, $p = 0.75$, $n = 5$, Fig. 6*Fa* and *Fc*). These results indicate that MAM-2201 presynaptically inhibits neurotransmitter release from CF terminals.

We then simultaneously recorded complex spikes in the somata and Ca^{2+} transients in the dendrites of PCs using the K-gluconate-based internal solution containing OGB-1 at near physiological temperature. Complex spikes were elicited under current-clamp conditions. As presented in Fig. 7*A*, electrical stimulation of CFs evoked all-or-none complex spikes consisting of spikelets (Control in Fig. 7*A*). MAM-2201 (10 μM, 10 min) significantly reduced the number of spikelets to 78% of the control (Fig. 7*B*, $n = 11$, $p < 0.001$). Because MAM-2201 modulated synaptic properties via activation of presynaptic CB1Rs (Fig. 3), and because PCs do not express CB1Rs (Kano et al., 2009), we would not expect MAM-2201 to affect the intrinsic membrane properties of PCs. As expected, we were able to confirm that MAM-2201 did not affect the resting membrane potential, input resistance, or action potential properties of PCs (Table 2). Accordingly, MAM-2201-induced changes in complex spike waveforms can be interpreted based on depression of CF-PC EPSCs. The complex spikes evoked by CF stimulation were accompanied by large Ca^{2+} transients in the dendrites (Fig. 7*Cb*, Control). MAM-2201 substantially decreased the peak amplitude of the Ca^{2+} transient (Fig. 7*Cb*, MAM-2201). Both the peak and the integral of the Ca^{2+} transients were significantly attenuated by 10 μM MAM-2201 (peak: $n = 10$, $p < 0.01$, Fig. 7*Da*; integration: $n = 10$, $p < 0.01$, Fig. 7*Db*). Taken together, these results indicate that MAM-2201 alters PC responses to CF activation by reducing the number of spikelets and the dendritic Ca^{2+} transients. This implies that MAM-2201 would decrease complex spike-mediated information propagation from PCs to the next nuclei and might affect induction of intracellular Ca^{2+}-dependent LTD at PF-PC synapses (see Discussion).

4. Discussion

This is the first study of the effects of MAM-2201 on neuronal functions. We found that MAM-2201 acted as an agonist of CB1Rs (Fig. 2). We also found that MAM-2201 inhibited glutamatergic synaptic transmission presynaptically via activation of presynaptic CB1Rs (Fig. 3). At the same concentrations, MAM-2201 decreased PF-PC EPSCs more potently than JWH-018 and Δ^9-THC (Fig. 4). Moreover, MAM-2201 also presynaptically suppressed GABAergic synaptic transmission at interneuron-PC synapses (Fig. 5) and glutamatergic synaptic transmission at CF-PC synapses (Fig. 6). In the case of smaller CF-PC EPSCs, MAM-2201 led to reduction of the number of action potentials in complex spikes and to reduced

dendritic intracellular Ca^{2+} transients (Fig. 7). Thus, it is likely that, in humans, the psychoactive effects caused by MAM-2201 are mainly due to inhibition of neurotransmitter release via activation of presynaptic CB1Rs.

4.1. The validity of our data on presynaptic inhibition at PF-PC synapses induced by synthetic cannabinoids

In our experiments, WIN reduced PF-PC EPSC amplitude to 64.5% (1 μM) and 46.8% (10 μM) of the control value using P20–57 mice (Fig. 4*D*). These reductions are comparable to previously published values obtained from acute cerebellar slice preparations: 55.6% of control in 1 μM WIN (P15–21 rats) (Levenes et al., 1998), 29.1 and 12.3% in 1 and 5 μM WIN, respectively (P15–19 rats) (Takahashi and Linden, 2000), and 23.5% in 5 μM WIN (P9–14 mice) (Kawamura et al., 2006). The latter two reports show somewhat smaller percentages compared with our data, but this can be attributed to the differences in the ages of the animals used: an immunohistochemical study revealed that the distribution patterns of CB1Rs in the molecular layer show developmental changes (Kawamura et al., 2006).

Atwood et al. reported that the IC50 of JWH-018 against synaptic transmission is 14.9 nM using autaptic hippocampal neuronal cultures (Atwood et al., 2010), whereas our IC50 value for JWH-018 was approximately 100 times larger than that of their report (Table 1). This discrepancy might be explained by the different neuronal preparations used: Atwood et al. utilized dissociated neuronal cultures, whose synapses would not be wrapped by cell structures such as glial membranes. These synapses would be more easily exposed to CB1R agonists compared with those in cerebellar slice preparations, and therefore synaptic transmission in the autaptic hippocampal cultures might be suppressed by a lower concentration of JWH-018.

Using a binding assay for human recombinant CB1Rs, we recently found that relative IC50s for WIN, MAM-2201, and JWH-018 against CB1Rs were 1.00, 0.70, and 5.30, respectively (Kikura-Hanajiri et al., manuscript in preparation). These data agree well with our observation of the relative IC50s against excitatory neurotransmitter release from PF terminals to PCs using cerebellar slice preparations (Table 1). Therefore, we consider our observations of IC50s in cerebellar preparations to be reasonable.

4.2. Adverse effects of MAM-2201 on targets of the cerebellar cortex and on cerebellum-dependent motor functions

PCs are the sole output GABAergic neurons from the cerebellar cortex and make direct synaptic contacts onto the deep cerebellar nuclear neurons and vestibular nuclear neurons (Voogd and Glickstein, 1998; Zheng and Raman, 2010). PCs receive two types of excitatory input from CFs and PFs. CFs arise from the inferior olivary complex located in the brainstem. CFs are activated during motor learning and induce complex spikes in PCs (Ito, 2001; Llinas et al., 2004). Spikelets in complex spike can propagate to the synaptic terminals of PCs (Khaliq and Raman, 2005). PFs are the axons of granule cells, which are excited by glutamatergic mossy fiber inputs. Mossy fibers originate from nuclei in the spinal cord and brain stem. The mossy fiber-PF pathway is the main operational input to the cerebellum and PCs, and carries afferent information both from the periphery and from other brain centers. PFs produce a brief excitatory postsynaptic potential in PCs that generates a single action potential called a “simple spike.” In addition, PCs receive feed-forward synaptic inhibition from GABAergic interneurons, and this inhibition increases the precision of PC spike outputs (Mittmann et al., 2005). Thus, all of these synaptic inputs to PCs can control the output of the cerebellar cortex. The absence of PC activity or genetic manipulation of synaptic transmission from PCs severely affects cerebellum-dependent motor functions: both in mutant mice and in spinocerebellar ataxia type 6 patients, selective degeneration of PCs induce motor dysfunction (Frontali, 2001; Porras-Garcia et al., 2013), and PC-specific vesicular GABA transporter knockout mice exhibit motor impairment (Kayakabe et al., 2013).

We demonstrate that MAM-2201 inhibits neurotransmitter release at PF-PC, interneuron-PC, and CF-PC synapses in a concentration-dependent manner (Figs. 3–6), and reduces the number of spikelets in CF-evoked complex spikes (Fig. 7*A* and *B*). Assuming that, in humans, MAM-2201 inhibits neurotransmitter release at these synapses, the inhibition at PF-PC synapses could cause failure of simple spike generation in PCs. The inhibition of interneuron-PC synapses may weaken the feed-forward inhibition, leading to decreased precision of PC spike outputs. MAM-2201-induced reduction of spikelets in complex spikes (Fig. 7*A* and *B*) could cause a decrease in the number of action potentials that propagate to the synaptic terminals of PCs. Consequently, MAM-2201 may interrupt normal GABAergic inhibition onto the deep cerebellar nuclear neurons and vestibular nuclear neurons, and thus could affect cerebellum-dependent motor coordination. This speculation could be supported by the report that consumption of drugs of abuse containing analogs of MAM-2201 can cause cerebellar dysfunction such as disturbance of finger-to-finger test (Musshoff et al., 2014).

4.3. Possible effects of MAM-2201 on cerebellar LTD initiated by dendritic Ca^{2+} transients and on motor learning functions

PF-PC LTD is thought to underlie cerebellar motor learning in mammals (Yuzaki, 2012). This learning is impaired in transgenic mice that exhibit a deficit in the expression of LTD *in vitro* (Kakegawa et al., 2008). Induction of LTD requires association of PF and CF activation both *in vivo* and *in vitro* (Ito, 2001). At the cellular level, CF synaptic inputs to PCs evoke dendritic Ca^{2+} transients, which play crucial roles in the expression of LTD (Konnerth et al., 1992). Interestingly, Carey and Regehr reported that presynaptic inhibition of CF-PC synapses by noradrenaline alters the complex spike waveform and decreases CF-evoked dendritic Ca^{2+} transients, leading to interference with the induction of LTD (Carey and Regehr, 2009). This noradrenergic modulation shares many features with our observations of MAM-2201-induced changes of CF-evoked responses in PCs (Figs. 6 and 7): depression of CF-PC EPSCs via presynaptic mechanisms, reduction of the number of spikelets in complex spikes, and attenuation of CF-induced Ca^{2+} transients in PC dendrites. Taken together, MAM-2201 may interfere with the induction of LTD *in vitro* and might result in an impairment of cerebellar motor learning *in vivo*. Further work will be needed to clarify whether MAM-2201 indeed blocks the induction of LTD.

4.4. Implications for adverse effects of MAM-2201 on other brain functions

In the brain, CB1Rs are widely and abundantly expressed, and numerous *in vitro* studies have revealed that activation of CB1Rs by agonists suppresses synaptic transmission in several regions such as the hippocampus, nucleus accumbens, striatum, and cerebellar cortex (Kano et al., 2009). Moreover, in rat hippocampal slice preparations, pharmacological activation of CB1Rs modulates long-term potentiation in the CA1 region (Navakkode and Korte, 2014), and *in vivo* administration of WIN impairs hippocampal-dependent short-term memory (Hampson and Deadwyler, 2000). WIN also activates the “reward circuitry” in the brain, including the ventral tegmental area-nucleus accumbens pathway, and alters reward-

related behaviors in a similar manner to other reward-enhancing addictive drugs (Gardner, 2005). In this study, we demonstrated that MAM-2201 suppresses synaptic transmission in the cerebellum and that this action parallels that induced by WIN (Figs. 3–5). Taken together, in humans, MAM-2201 could cause psychoactive effects that are similar to those observed in the laboratory animal experiments using WIN or other synthetic cannabinoids.

Acknowledgments

This work was supported by Health Labour Sciences Research Grants. We thank Dr. Nobutake Hosoi (Gunma University) for technical advice on intracellular Ca^{2+} imaging.

References

Atwood, B.K., Huffman, J., Straiker, A., Mackie, K., 2010. JWH018, a common constituent of 'Spice' herbal blends, is a potent and efficacious cannabinoid CB receptor agonist. Br. J. Pharmacol. 160, 585–593.
Auwarter, V., Dresen, S., Weinmann, W., Muller, M., Putz, M., Ferreiros, N., 2009. 'Spice' and other herbal blends: harmless incense or cannabinoid designer drugs? J. Mass Spectrom. 44, 832–837.
Brown, S.P., Safo, P.K., Regehr, W.G., 2004. Endocannabinoids inhibit transmission at granule cell to Purkinje cell synapses by modulating three types of presynaptic calcium channels. J. Neurosci. 24, 5623–5631.
Bruno, A., Lembo, F., Novellino, E., Stornaiuolo, M., Marinelli, L., 2014. Beyond radiodisplacement techniques for identification of CB1 ligands: the first application of a fluorescence-quenching assay. Sci. Rep. 4, 3757.
Carey, M.R., Regehr, W.G., 2009. Noradrenergic control of associative synaptic plasticity by selective modulation of instructive signals. Neuron 62, 112–122.
Derungs, A., Schwaninger, A.E., Mansella, G., Bingisser, R., Kraemer, T., Liechti, M.E., 2013. Symptoms, toxicities, and analytical results for a patient after smoking herbs containing the novel synthetic cannabinoid MAM-2201. Forensic Toxicol. 31, 164–171.
DeSanty, K.P., Dar, M.S., 2001. Cannabinoid-induced motor incoordination through the cerebellar CB(1) receptor in mice. Pharmacol. Biochem. Behav. 69, 251–259.
Diana, M.A., Levenes, C., Mackie, K., Marty, A., 2002. Short-term retrograde inhibition of GABAergic synaptic currents in rat Purkinje cells is mediated by endogenous cannabinoids. J. Neurosci. 22, 200–208.
Dousmanis, A.G., Pennefather, P.S., 1992. Inwardly rectifying potassium conductances in AtT-20 clonal pituitary cells. Pflugers Arch. 422, 98–104.
Felder, C.C., Joyce, K.E., Briley, E.M., Glass, M., Mackie, K.P., Fahey, K.J., Cullinan, G.J., Hunden, D.C., Johnson, D.W., Chaney, M.O., Koppel, G.A., Brownstein, M., 1998. LY320135, a novel cannabinoid CB1 receptor antagonist, unmasks coupling of the CB1 receptor to stimulation of cAMP accumulation. J. Pharmacol. Exp. Ther. 284, 291–297.
Frontali, M., 2001. Spinocerebellar ataxia type 6: channelopathy or glutamine repeat disorder? Brain Res. Bull. 56, 227–231.
Gardner, E.L., 2005. Endocannabinoid signaling system and brain reward: emphasis on dopamine. Pharmacol. Biochem. Behav. 81, 263–284.
Hagiwara, S., Miyazaki, S., Rosenthal, N.P., 1976. Potassium current and the effect of cesium on this current during anomalous rectification of the egg cell membrane of a starfish. J. Gen. Physiol. 67, 621–638.
Hampson, R.E., Deadwyler, S.A., 2000. Cannabinoids reveal the necessity of hippocampal neural encoding for short-term memory in rats. J. Neurosci. 20, 8932–8942.
Hashimoto, K., Kano, M., 2013. Synapse elimination in the developing cerebellum. Cell. Mol. Life Sci. 70, 4667–4680.
Huestis, M.A., Gorelick, D.A., Heishman, S.J., Preston, K.L., Nelson, R.A., Moolchan, E.T., Frank, R.A., 2001. Blockade of effects of smoked marijuana by the CB1-selective cannabinoid receptor antagonist SR141716. Arch. Gen. Psychiatry 58, 322–328.
Irie, T., Fukui, I., Ohmori, H., 2006. Activation of GIRK channels by muscarinic receptors and group II metabotropic glutamate receptors suppresses Golgi cell activity in the cochlear nucleus of mice. J. Neurophysiol. 96, 2633–2644.
Irie, T., Matsuzaki, Y., Sekino, Y., Hirai, H., 2014. Kv3.3 channels harbouring a mutation of spinocerebellar ataxia type 13 alter excitability and induce cell death in cultured cerebellar Purkinje cells. J. Physiol. 592, 229–247.
Irie, T., Ohmori, H., 2008. Presynaptic GABA(B) receptors modulate synaptic facilitation and depression at distinct synapses in fusiform cells of mouse dorsal cochlear nucleus. Biochem. Biophys. Res. Commun. 367, 503–508.
Ito, M., 2001. Cerebellar long-term depression: characterization, signal transduction, and functional roles. Physiol. Rev. 81, 1143–1195.
Kakegawa, W., Miyazaki, T., Emi, K., Matsuda, K., Kohda, K., Motohashi, J., Mishina, M., Kawahara, S., Watanabe, M., Yuzaki, M., 2008. Differential regulation of synaptic plasticity and cerebellar motor learning by the C-terminal PDZ-binding motif of GluRdelta2. J. Neurosci. 28, 1460–1468.
Kano, M., Ohno-Shosaku, T., Hashimotodani, Y., Uchigashima, M., Watanabe, M., 2009. Endocannabinoid-mediated control of synaptic transmission. Physiol. Rev. 89, 309–380.
Kawamura, Y., Fukaya, M., Maejima, T., Yoshida, T., Miura, E., Watanabe, M., Ohno-Shosaku, T., Kano, M., 2006. The CB1 cannabinoid receptor is the major cannabinoid receptor at excitatory presynaptic sites in the hippocampus and cerebellum. J. Neurosci. 26, 2991–3001.
Kayakabe, M., Kakizaki, T., Kaneko, R., Sasaki, A., Nakazato, Y., Shibasaki, K., Ishizaki, Y., Saito, H., Suzuki, N., Furuya, N., Yanagawa, Y., 2013. Motor dysfunction in cerebellar Purkinje cell-specific vesicular GABA transporter knockout mice. Front. Cell. Neurosci. 7, 286.
Khaliq, Z.M., Raman, I.M., 2005. Axonal propagation of simple and complex spikes in cerebellar Purkinje neurons. J. Neurosci. 25, 454–463.
Kikura-Hanajiri, R., Uchiyama, N., Kawamura, M., Goda, Y., 2013. Changes in the prevalence of new psychoactive substances before and after the introduction of the generic scheduling of synthetic cannabinoids in Japan. Drug Test. Anal..
Konnerth, A., Dreessen, J., Augustine, G.J., 1992. Brief dendritic calcium signals initiate long-lasting synaptic depression in cerebellar Purkinje cells. Proc. Natl. Acad. Sci. U. S. A. 89, 7051–7055.
Korn, H., Faber, D.S., 1991. Quantal analysis and synaptic efficacy in the CNS. Trends Neurosci. 14, 439–445.
Kreitzer, A.C., Regehr, W.G., 2001. Retrograde inhibition of presynaptic calcium influx by endogenous cannabinoids at excitatory synapses onto Purkinje cells. Neuron 29, 717–727.
Kubo, Y., Reuveny, E., Slesinger, P.A., Jan, Y.N., Jan, L.Y., 1993. Primary structure and functional expression of a rat G-protein-coupled muscarinic potassium channel. Nature 364, 802–806.
Kushmerick, C., Price, G.D., Taschenberger, H., Puente, N., Renden, R., Wadiche, J.I., Duvoisin, R.M., Grandes, P., von Gersdorff, H., 2004. Retroinhibition of presynaptic Ca^{2+} currents by endocannabinoids released via postsynaptic mGluR activation at a calyx synapse. J. Neurosci. 24, 5955–5965.
Levenes, C., Daniel, H., Soubrie, P., Crepel, F., 1998. Cannabinoids decrease excitatory synaptic transmission and impair long-term depression in rat cerebellar Purkinje cells. J. Physiol. 510 (Pt 3), 867–879.
Llinas, R., Walton, K.D., Lang, E.J., 2004. Cerebellum. In: Shepard, G.M. (Ed.), The Synaptic Organization of the Brain, fifth ed. Oxford University Press, New York, NY, US, pp. 271–309.
Lonati, D., Buscaglia, E., Papa, P., Valli, A., Coccini, T., Giampreti, A., Petrolini, V.M., Vecchio, S., Serpelloni, G., Locatelli, C.A., 2014. MAM-2201 (analytically confirmed) intoxication after "synthacaine" consumption. Ann. Emerg. Med..
Luk, T., Jin, W., Zvonok, A., Lu, D., Lin, X.Z., Chavkin, C., Makriyannis, A., Mackie, K., 2004. Identification of a potent and highly efficacious, yet slowly desensitizing CB1 cannabinoid receptor agonist. Br. J. Pharmacol. 142, 495–500.
Mackie, K., 2008. Signaling via CNS cannabinoid receptors. Mol. Cell. Endocrinol. 286, S60–S65.
Mackie, K., Lai, Y., Westenbroek, R., Mitchell, R., 1995. Cannabinoids activate an inwardly rectifying potassium conductance and inhibit Q-type calcium currents in AtT20 cells transfected with rat brain cannabinoid receptor. J. Neurosci. 15, 6552–6561.
Maejima, T., Hashimoto, K., Yoshida, T., Aiba, A., Kano, M., 2001. Presynaptic inhibition caused by retrograde signal from metabotropic glutamate to cannabinoid receptors. Neuron 31, 463–475.
McKay, B.E., Turner, R.W., 2005. Physiological and morphological development of the rat cerebellar Purkinje cell. J. Physiol. 567, 829–850.
Mittmann, W., Koch, U., Hausser, M., 2005. Feed-forward inhibition shapes the spike output of cerebellar Purkinje cells. J. Physiol. 563, 369–378.
Monory, K., Blaudzun, H., Massa, F., Kaiser, N., Lemberger, T., Schutz, G., Wotjak, C.T., Lutz, B., Marsicano, G., 2007. Genetic dissection of behavioural and autonomic effects of Delta(9)-tetrahydrocannabinol in mice. PLoS Biol. 5, e269.
Moosmann, B., Kneisel, S., Girreser, U., Brecht, V., Westphal, F., Auwarter, V., 2012. Separation and structural characterization of the synthetic cannabinoids JWH-412 and 1-[(5-fluoropentyl)-1H-indol-3yl]-(4-methylnaphthalen-1-yl)methanone using GC-MS, NMR analysis and a flash chromatography system. Forensic Sci. Int. 220, e17–22.
Musshoff, F., Madea, B., Kernbach-Wighton, G., Bicker, W., Kneisel, S., Hutter, M., Auwarter, V., 2014. Driving under the influence of synthetic cannabinoids ("Spice"): a case series. Int. J. Legal Med. 128, 59–64.
Navakkode, S., Korte, M., 2014. Pharmacological activation of CB1 receptor modulates long term potentiation by interfering with protein synthesis. Neuropharmacology 79, 525–533.
Patel, S., Hillard, C.J., 2001. Cannabinoid CB(1) receptor agonists produce cerebellar dysfunction in mice. J. Pharmacol. Exp. Ther. 297, 629–637.
Porras-Garcia, M.E., Ruiz, R., Perez-Villegas, E.M., Armengol, J.A., 2013. Motor learning of mice lacking cerebellar Purkinje cells. Front. Neuroanat. 7, 4.
Regehr, W.G., Carey, M.R., Best, A.R., 2009. Activity-dependent regulation of synapses by retrograde messengers. Neuron 63, 154–170.
Safo, P.K., Cravatt, B.F., Regehr, W.G., 2006. Retrograde endocannabinoid signaling in the cerebellar cortex. Cerebellum 5, 134–145.
Safo, P.K., Regehr, W.G., 2005. Endocannabinoids control the induction of cerebellar LTD. Neuron 48, 647–659.
Saito, T., Namera, A., Miura, N., Ohta, S., Miyazaki, S., Osawa, M., Inokuchi, S., 2013. A fatal case of MAM-2201 poisoning. Forensic Toxicol. 31, 333–337.
Seely, K.A., Lapoint, J., Moran, J.H., Fattore, L., 2012. Spice drugs are more than harmless herbal blends: a review of the pharmacology and toxicology of synthetic cannabinoids. Prog. Neuro Psychopharmacol. Biol. Psychiatry 39, 234–243.

Shen, M., Thayer, S.A., 1999. Delta9-tetrahydrocannabinol acts as a partial agonist to modulate glutamatergic synaptic transmission between rat hippocampal neurons in culture. Mol. Pharmacol. 55, 8–13.
Showalter, V.M., Compton, D.R., Martin, B.R., Abood, M.E., 1996. Evaluation of binding in a transfected cell line expressing a peripheral cannabinoid receptor (CB2): identification of cannabinoid receptor subtype selective ligands. J. Pharmacol. Exp. Ther. 278, 989–999.
Shuvaev, A.N., Horiuchi, H., Seki, T., Goenawan, H., Irie, T., Iizuka, A., Sakai, N., Hirai, H., 2011. Mutant PKC{gamma} in spinocerebellar ataxia type 14 disrupts synapse elimination and long-term depression in Purkinje cells in vivo. J. Neurosci. 31, 14324–14334.
Szabo, B., Than, M., Thorn, D., Wallmichrath, I., 2004. Analysis of the effects of cannabinoids on synaptic transmission between basket and Purkinje cells in the cerebellar cortex of the rat. J. Pharmacol. Exp. Ther. 310, 915–925.
Takahashi, K.A., Linden, D.J., 2000. Cannabinoid receptor modulation of synapses received by cerebellar Purkinje cells. J. Neurophysiol. 83, 1167–1180.
Taura, F., Sirikantaramas, S., Shoyama, Y., Shoyama, Y., Morimoto, S., 2007. Phytocannabinoids in Cannabis sativa: recent studies on biosynthetic enzymes. Chem. Biodivers. 4, 1649–1663.
Uchiyama, N., Kawamura, M., Kikura-Hanajiri, R., Goda, Y., 2013. URB-754: a new class of designer drug and 12 synthetic cannabinoids detected in illegal products. Forensic Sci. Int. 227, 21–32.
Vardakou, I., Pistos, C., Spiliopoulou, C., 2010. Spice drugs as a new trend: mode of action, identification and legislation. Toxicol. Lett. 197, 157–162.
Vincent, P., Marty, A., 1996. Fluctuations of inhibitory postsynaptic currents in Purkinje cells from rat cerebellar slices. J. Physiol. 494 (Pt 1), 183–199.
Voogd, J., Glickstein, M., 1998. The anatomy of the cerebellum. Trends Cogn. Sci. 2, 307–313.
Wilson, R.I., Nicoll, R.A., 2002. Endocannabinoid signaling in the brain. Science 296, 678–682.
Xu-Friedman, M.A., Regehr, W.G., 1999. Presynaptic strontium dynamics and synaptic transmission. Biophys. J. 76, 2029–2042.
Yuzaki, M., 2012. Cerebellar LTD vs. motor learning-lessons learned from studying GluD2. Neural Netw..
Zheng, N., Raman, I.M., 2010. Synaptic inhibition, excitation, and plasticity in neurons of the cerebellar nuclei. Cerebellum 9, 56–66.
Zucker, R.S., Regehr, W.G., 2002. Short-term synaptic plasticity. Annu Rev. Physiol. 64, 355–405.